



HAL
open science

Solid-solution (alloying) strategies in crystalline molecular conductors

Marc Fourmigue

► **To cite this version:**

Marc Fourmigue. Solid-solution (alloying) strategies in crystalline molecular conductors. *Journal of Materials Chemistry C*, 2021, 9, pp.10557-10572. 10.1039/d1tc02160e . hal-03330996

HAL Id: hal-03330996

<https://hal.science/hal-03330996>

Submitted on 15 Sep 2021

HAL is a multi-disciplinary open access archive for the deposit and dissemination of scientific research documents, whether they are published or not. The documents may come from teaching and research institutions in France or abroad, or from public or private research centers.

L'archive ouverte pluridisciplinaire **HAL**, est destinée au dépôt et à la diffusion de documents scientifiques de niveau recherche, publiés ou non, émanant des établissements d'enseignement et de recherche français ou étrangers, des laboratoires publics ou privés.

Solid-solution (alloying) strategies in crystalline molecular conductors

Marc Fourmigué

Univ Rennes, CNRS, ISCR (Institut des Sciences Chimiques de Rennes), UMR 6226, Campus de Beaulieu, 35000 Rennes, France

Abstract

In this review, we describe solid solutions strategies employed in molecular conductors, where the control of the transport and magnetic properties (metallic or superconducting behavior, metal-insulator transitions, etc) is the main goal. We first describe the main features of molecular conductors in order to identify which molecular entities are prone to be substituted by others in solid solutions, to which extend and for which purpose. We then describe the different crystal growth techniques used toward solid solutions elaboration and the nature of the molecular species, electroactive or not, which have been used, in cation or anion radical salts, in charge transfer salts or in single component conductors, in more than sixty reported examples. Topics such as preferential insertion and miscibility, nature of disorder and the different analytical tools used for characterizing these alloys will be presented. The consequences of alloying on conductivity and on phase transitions (superconductivity, anion ordering, Peierls, Spin-Peierls), the concepts of chemical pressure effects, band filling manipulation, π -d interactions with magnetic anions will be also discussed.

1 Introduction

Engineering crystal properties through solid solutions offers an opportunity to fine-tune the structural and physico-chemical properties of molecular materials, with in some cases, apparition of novel, unexpected behaviors. As stated by Lusi,¹ a plethora of terms has been used over the years to define what we called indiscriminately solid solutions or alloys. They can be defined as multi-component phases for which the component ratios can be varied in continuum. They differ in that respect from salts or co-crystals where the stoichiometry defines the exact composition expressed by integer ratios (1:2, 1:3, 1:2:1, etc).² Solid solutions offer therefore a high potential for tuning molecular properties in a smooth and controlled way, over a broad range of compositions. Working with *molecular* solid solutions also induces a notable

difference with the well-known inorganic alloys such as steel (Fe + C), brass (Zn + Cu), binary ($\text{Si}_x\text{Ge}_{1-x}$) or ternary ($\text{In}_x\text{Ga}_{1-x}\text{As}$) semiconductors built out of atomic constituents which are held by strong covalent bonds.³ Interactions between molecules in molecular solids are usually much weaker and molecular entities keep their integrity in the solid. Note however that in organic conductors, metallic bonding can play an important role to control the overall solid-state arrangement. In the following, we will restrict ourselves to crystalline, single-phase materials and will not consider molecular amorphous blends as used for example in molecular semiconductors,³ or crystals grown on crystals through stepwise 3D epitaxial growth.⁴

The more general question of the effect of disorder in molecular alloys has been addressed from a thermodynamic point of view as respect to the effect of an increased entropy.⁵ Several entropic effects can be considered in molecular crystals, which are referred as to configurational entropy, vibrational entropy and rotational entropy. Configurational entropy can be found because of molecular disorder (one molecule or a part of a molecule disordered on two or more sites), eventually associated with temperature-dependent molecular motions and thermal expansion behaviors.⁶ In solid solutions of molecular compounds, the nature of the disorder (*vs.* clustering or spinodal decomposition) can play an important role, as shown recently in $\text{CH}_3\text{NH}_3\text{PbI}_3/\text{CH}_3\text{NH}_3\text{PbBr}_3$ alloys of hybrid halide perovskite semiconductors used for photovoltaic applications.⁷ Furthermore, in addition to static substitutional disorder that arises from molecular substitution, orientational disorder on a given site can also play a role, with two isomorphous molecules or ions adopting different orientations.⁸ Another difficulty one can encounter is the situation when co-crystallization of similar molecules does not, as previously believed, necessarily result in the formation of macroscopic crystals with the same homogeneous distribution of components.⁹ This effect, observed in $[\text{M}_x\text{M}'_{1-x}(\text{bipy})_3](\text{PF}_6)_2$ (M , $\text{M}' = \text{Ni}^{2+}, \text{Fe}^{2+}, \text{Ru}^{2+}$; bipy: 2,2'-bipyridine) solid solutions, gives rise to crystals from the same batch with composition varying notably (by as much as 15%) from the averaged composition. This effect described as supramolecular selectivity is explained by molecular recognition processes that lead to the partially selective aggregation of like molecules. These lines illustrate how difficult the full characterization of molecular solid solutions can be. For most reported examples detailed below, many of these questions about the nature of the disorder, the exact composition and structure of the crystals, their homogeneity, were never addressed, limiting in some extent the conclusions that many authors draw on the correlation between alloy composition and physical properties.

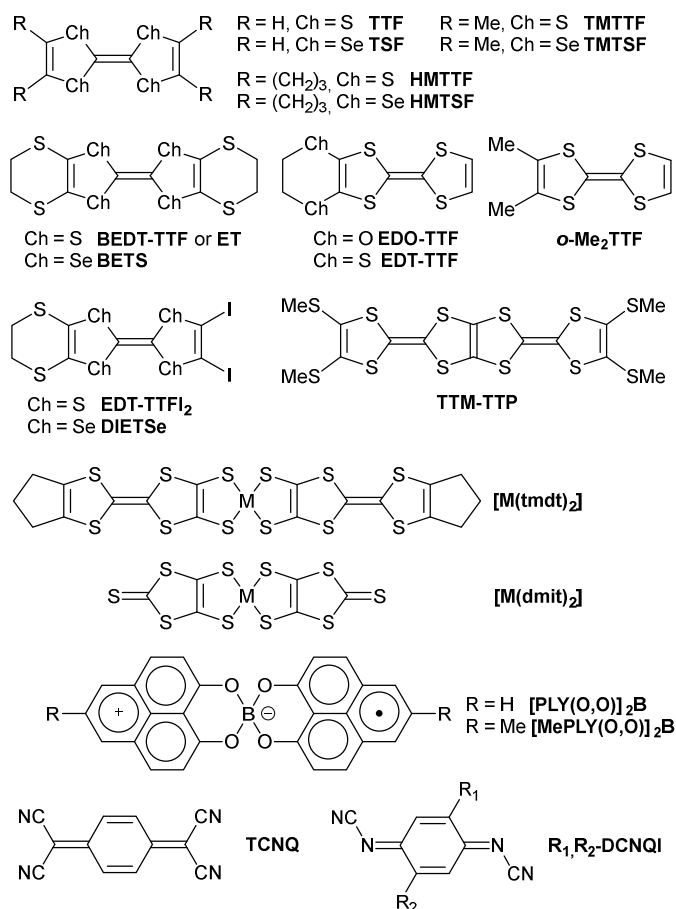
In molecular materials, solid solutions strategies are used extensively to control different properties, such as magnetism, luminescence, or catalysis. The molecular magnetism community makes an extensive use of alloying strategies. This is particularly true in coordination complexes exhibiting spin crossover (SCO) behavior. Substitution of counterion (for example PF_6^- vs. AsF_6^-) or ligand, dilution of the magnetic center by other cations can have very important consequences on the cooperativity of the SCO and eventual presence of structural phase transitions.^{10,11,12} Another striking example involves the modulation of Single Molecule Magnet (SMM) properties of pentadecanuclear cyanide-bridged clusters formulated as $\{\text{Fe}_{9-x}\text{Co}_x[\text{W}(\text{CN})_8]_6(\text{MeOH})_{24}\}$, where different Co/Fe metal ratios favor either $^{\text{HS}}\text{Fe}^{\text{II}} \text{W}^{\text{V}} \leftrightarrow ^{\text{HS}}\text{Fe}^{\text{III}} \text{W}^{\text{IV}}$ charge transfer transition or slow magnetic relaxation effects.¹³ Luminescent species, particularly those based on rare-earth complexes offer another playground for alloying strategies. For example, lanthanide complexes of the 5-methoxyisophthalate (mip^{2-}) ligand, formulated as $[\text{Ln}_2(\text{mip})_3(\text{H}_2\text{O})_8 \cdot 4\text{H}_2\text{O}]$ are prepared with a mixture of up to six different lanthanide ions (Nd^{3+} , Sm^{3+} , Eu^{3+} , Gd^{3+} , Tb^{3+} , Dy^{3+}). Under a unique irradiation wavelength ($\lambda_{\text{exc}} = 325 \text{ nm}$), this compound exhibits almost 20 emission peaks in both visible and NIR regions at RT, an unprecedented richness of the emission spectrum of great interest as far as luminescent barcodes are targeted.¹⁴ The chemistry of Metal Organic Frameworks (MOF) also provides several examples of successful alloying strategies, as those reported to tune catalytic properties by virtue of the $\text{In}^{3+}/\text{Ga}^{3+}$ metal ions ratio,¹⁵ or to manipulate the mechanical and dynamical properties of formate-based perovskites in the series $[\text{NH}_3\text{NH}_2]_{1-x}[\text{NH}_3\text{OH}]_x\text{Zn}(\text{HCOO})_3$.¹⁶

In this review, we will focus ourselves on solid solutions strategies employed in molecular conductors, where the control of the transport properties (metallic or superconducting behavior, metal-insulator transitions with associated magnetic properties) is the main goal. To do so, it is important to first describe the main features of molecular conductors in order to identify which molecular entities are prone to be substituted by others in solid solutions and for which purpose.

The term “molecular conductors” encompasses, within this review, a broad range of crystalline materials built out of molecular entities, be they from organic or coordination chemistry origin, able to generate charge carriers. Intermolecular interactions in the solid state, most often of 1D or 2D nature, favors the formation of bands, with a limited gap in semiconducting systems ($\approx 10^{-4} \text{ S cm}^{-1} < \sigma_{\text{RT}} < \approx 1 \text{ S cm}^{-1}$), and a limited bandwidth in gapless metallic systems ($\sigma_{\text{RT}} > \approx 1 \text{ S cm}^{-1}$). These characteristics are the consequence of strong electronic correlations between charge carriers,¹⁷ and offer a wide variety of ground states and

phase transitions, referred as Charge Density Wave (CDW), Spin Density Wave (SDW), Peierls, Spin-Peierls (SP), Dimer-Mott (DM), Mott-insulator, Charge-Order (CO), superconductivity, etc.¹⁸ From a composition point of view, we can distinguish three main different classes of compounds, each of them amenable to different solid solution strategies.

Charge-transfer salts are based on the association of two different electroactive molecules, one referred as the electron donor (D) and one referred as the electron acceptor (A). Upon co-crystallization from solution or from co-sublimation, the D•A co-crystal is formed and its electronic nature varies with the $E^{1/2}$ redox potentials of both D and A molecules.¹⁹ While in solution, electron transfer can occur if $E_{\text{red}}(\text{A}) > E_{\text{ox}}(\text{D})$, formation of a crystalline solid favors ionic phases and electron transfer can be observed if $E_{\text{red}}(\text{A}) - E_{\text{ox}}(\text{D}) > -(0.25-035)$ V. A partial degree of charge transfer, $0 < \rho < 1$, is found in segregated structures with DDD and AAA stacks, as in $\text{TTF}^{+\rho} \cdot \text{TCNQ}^{-\rho}$ (Scheme 1),²⁰ where the Fermi level crosses both HOMO band of D and LUMO band of A, at the origin of the metallic character. Solid solutions can be considered within such charge-transfer salts by replacing either D or A by an isomorphous molecule, i.e. $(\text{D}_x\text{D}'_{1-x}) \cdot \text{A}$ or $\text{D} \cdot (\text{A}_x\text{A}'_{1-x})$.



Scheme 1 Electroactive molecules involved in solid solutions

Ion-radical salts are based on one single electroactive molecule (either D or A), respectively oxidized or reduced in the radical cation $D^{\bullet+}$ or radical anion $A^{\bullet-}$ form. Partial charge transfer is also possible, for example with the recurrent 2:1 stoichiometry in $(D)_2^{\bullet}X$ ($\rho = 0.5$ if X is a monovalent anion). More complex situations are found in systems like $(D)_3^{\bullet}X_2$ or with non-stoichiometric band filling,²¹ as in TTF halides $(TTF)X_x$ ($x = 0.77-0.80$ with Cl^- , $x = 0.71-0.76$ with Br^- and $x = 0.70-0.72$ for I^-).²² The Fabre salts (2:1 salts built out of TMTTF molecules), the Bechgaard salts (2:1 salts built out of TMTSF molecules),¹⁸ and the large family of BEDT-TTF salts²³ (and BETS and BET analogs)^{24,25} belong to this class of molecular conductors. Solid solutions here can take on different aspects, by replacing the electroactive molecule by an isomorphous one as in charge-transfer salts, i.e. $(D_xD'_{1-x})_nX$, or by replacing the counter-ion by an isomorphous one, i.e. $D_n(X_xY_{1-x})$. If X and Y differ in charge, band filling will be also impacted, a difficult but sought-after goal, as we will see in the following.

Single component conductors are built from one single molecular species, be it radical in nature or not. Among organic radical species, we can mention the spiro-bis(phenalenyl)boron radicals,²⁶ the dithiadiazolyl,²⁷ or dithiazolyl radicals,²⁸ hydrogen-bonded TTF dimers.^{29,30} Among coordination complexes, the most famous series is based on neutral tetrathiafulvalene dithiolate complexes such as $[M(tmdt)_2]$,³¹ while neutral radical gold complexes such as $[Au(R-thiazdt)_2]^{\bullet}$ emerged as an attractive family.³² In-between we can find neutral nickel bis(dithiolene) complexes whose semiconducting behavior can be changed into a metallic one under application of high pressures.³³ Among all these single-component conductors, alloying strategies have been considered up to now only upon metal substitution, in spiro-bis(phenalenyl)boron radicals (B vs. Be) and in the TTF-dithiolate complexes (M = Ni, Pd, Pt vs. Cu, Au).

Reported solid solutions of molecular conductors analyzed in this Review have been gathered in Tables 1 and 2, distinguishing those involving alloys based on the electroactive molecules (Table 1) and those involving alloys based on the counter-ions (Table 2).

Table 1 Reported solid solutions of molecular conductors based on different electroactive donor or acceptor molecules.

Compound	Mixed D or A molecule	Composition	Ref
<i>Charge-transfer salts:</i>			
(TSF) _x (TTF) _{1-x} (TCNQ)	TTF, TSF	0 ≤ x ≤ 1	34,35,36
(HMTSF) _{1-x} (HMTTF) _x TCNQ	HMTTF, HMTSF	0.05	37
(NMP) _x (Phen) _{1-x} TCNQ	NMP, Phen	0.5 ≤ x ≤ 1	38,39
<i>Cation-radical salts:</i>			
[(TMTSF) _{1-x} (TMTTF) _x] ₂ ClO ₄	TMTTF, TMTSF	0 ≤ x ≤ 0.30	40
[(TMTSF) _{1-x} (TMTTF) _x] ₂ ReO ₄	TMTTF, TMTSF	0 ≤ x ≤ 1	41,42
[(TMTSF) _{1-x} (TMTTF) _x] ₂ PF ₆	TMTTF, TMTSF	x < 0.25, 0.85	43
κ-[(ET) _{1-x} (BEDT-STF) _x] ₂	BEDT-TTF,	0 ≤ x ≤ 1	44
Cu[N(CN) ₂]Br	BEDT-STF		
κ-[(ET) _{1-x} (BEDSeT-TTF) _x] ₂	BEDT-TTF,	0 ≤ x ≤ 0.26	45
Cu[N(CN) ₂]Br	BEDSeT-TTF		
[(EDO-TTF) _{1-x} (MeEDO-TTF) _x] ₂ PF ₆	EDO-TTF, MeEDO-TTF	x < 0.6, 0.9 < x	46
(Perylene) ₂ [Au _{1-x} Pt _x (mnt) ₂]	Au ³⁺ , Pt ²⁺	0 ≤ x ≤ 0.50	47,48,49
<i>Single component conductors:</i>			
[NiOC ₄] _{1-x} [AuOC ₄] _x	Ni ²⁺ , Au ³⁺	0 ≤ x ≤ 1	50
[Ni _{1-x} Au _x (tmdt) ₂]	Ni ²⁺ , Au ³⁺	0 ≤ x ≤ 1	51
[Ni _{1-x} Cu _x (tmdt) ₂]	Ni ²⁺ , Cu ²⁺	x ≤ 0.27	52
[PLY(O,O)] ₂ B _{1-x} Be _x	B ³⁺ , Be ²⁺	0 ≤ x ≤ 0.2	53
[MePLY(O,O)] ₂ B _{1-x} Be _x	B ³⁺ , Be ²⁺	0 ≤ x ≤ 0.59	54
<i>Anion-radical salts:</i>			
[Cl-BzPy][Ni _x Pt _{1-x} (mnt) ₂]	Ni ²⁺ , Pt ²⁺	0 ≤ x ≤ 1	55
[NO ₂ -BzPy][Ni _x Au _{1-x} (mnt) ₂]	Ni ²⁺ , Au ²⁺	0 ≤ x ≤ 1	56
(Me ₄ N)[Ni _x Pd _{1-x} (dmit) ₂]	Ni ²⁺ , Pd ²⁺		57
[(Me ₂ DCNQI) _{1-x} (Me ₂ DCNQI-d ₈) _x] ₂ Cu	Me ₂ DCNQI, Me ₂ DCNQI-d ₈	0 ≤ x ≤ 1	58,61
[(Me ₂) _{1-x} (MeBr) _x DCNQI] ₂ Cu	Me ₂ DCNQI, MeBrDCNQI	0 ≤ x ≤ 1	59,60,61
[(Me ₂) _{1-x} (MeCl) _x DCNQI] ₂ Cu	Me ₂ DCNQI, MeClDCNQI	0.75	62
[(Me ₂) _{1-x} (MeI) _x DCNQI] ₂ Cu	Me ₂ DCNQI, MeIDCNQI	0.70	62,61
[(MeCl) _{1-x} (MeBr) _x DCNQI] ₂ Cu	MeClDCNQI, MeBrDCNQI	0.60	62
[(MeBr) _{1-x} (MeI) _x DCNQI] ₂ Cu	MeBrDCNQI, MeIDCNQI	0 ≤ x ≤ 1	62,61
[(MeCl) _{1-x} (MeI) _x DCNQI] ₂ Cu	MeClDCNQI, MeIDCNQI	0.25	62
K ₃ (C ₆₀) _{1-x} (C ₇₀) _x	C ₆₀ , C ₇₀		63
TDAE•(C ₆₀) _{1-x} (C ₇₀) _x	C ₆₀ , C ₇₀	0 ≤ x ≤ 0.5	64

Table 2 Reported solid solutions of molecular conductors based on different counter-ions

Compound	Mixed counter-ions	Composition	Ref
<i>Anion radical salts:</i>			
(Me ₂ DCNQI) ₂ Li _{1-x} Cu _x	Li ⁺ , Cu ^{+,2+}	0 ≤ x ≤ 1	65,66
(Me ₄ Sb) _{1-x} (EtMe ₃ Sb) _x [Pd(dmit) ₂] ₂	Me ₄ Sb ⁺ , EtMe ₃ Sb ⁺	0 ≤ x ≤ 1	67
(Et ₂ Me ₂ Sb) _{1-x} (EtMe ₃ Sb) _x [Pd(dmit) ₂] ₂	Et ₂ Me ₂ Sb ⁺ , EtMe ₃ Sb ⁺	0 ≤ x ≤ 1	67
<i>Cation-radical salts:</i>			
(<i>o</i> -DMTTF) ₂ Br _x Cl _{1-x}	Br ⁻ , Cl ⁻	0 ≤ x ≤ 1	68
(<i>o</i> -DMTTF) ₂ Br _x I _{1-x}	Br ⁻ , I ⁻	0 ≤ x ≤ 1	68
(TMTSF) ₂ (ClO ₄) _{1-x} (ReO ₄) _x	ClO ₄ ⁻ , ReO ₄ ⁻	x < 0.17	69,70,71,72
(TMTSF) ₂ (AsF ₆) _{1-x} (FeCl ₄) _x	AsF ₆ ⁻ , FeCl ₄ ⁻	10 ⁻³	73
(TMTTF) ₂ (SbF ₆) _{1-x} (AsF ₆) _x	AsF ₆ ⁻ , SbF ₆ ⁻	0 ≤ x ≤ 1	74,75
(TMTSF) ₂ (TaF ₆) _{1-x} (PF ₆) _x	TaF ₆ ⁻ , PF ₆ ⁻	0 ≤ x ≤ 1	76
δ _m -(BEDT-TTF) ₂ (TaF ₆) _{1-x} (PF ₆) _x	TaF ₆ ⁻ , PF ₆ ⁻	0.06	76
δ _o -(BEDT-TTF) ₂ (TaF ₆) _{1-x} (PF ₆) _x	TaF ₆ ⁻ , PF ₆ ⁻	0.57	76
β-(ET) ₂ (I ₃) _{1-x} (IBr ₂) _x	IBr ₂ ⁻ , I ₃ ⁻	0 ≤ x ≤ 1	77,78
β-(ET) ₂ (IBr ₂) _{1-x} (I ₂ Br) _x	IBr ₂ ⁻ , I ₂ Br ⁻	0 ≤ x ≤ 1	77,78
β-(ET) ₂ (I ₂ Br) _{1-x} (I ₃) _x	I ₂ Br ⁻ , I ₃ ⁻	0 ≤ x ≤ 1	77,78
β-(ET) ₂ (I ₃) _{1-x} (AuI ₂) _x	AuI ₂ ⁻ , I ₃ ⁻	0.1, 0.26, 0.9	79,80
θ-(ET) ₂ (I ₃) _{1-x} (AuI ₂) _x	AuI ₂ ⁻ , I ₃ ⁻	< 0.02	81
(ET) ₄ [Ni(CN) ₄] _x [Pt(CN) ₄] _{1-x}	[Ni(CN) ₄] ²⁻ , [Pt(CN) ₄] ²⁻	≈0.5, 0.14	82
κ-(ET) ₂ Cu[N(CN) ₂] ₂ Br _x Cl _{1-x}	Cl ⁻ , Br ⁻	0 ≤ x ≤ 1	83,84,85
θ-(ET) ₂ (Rb _{1-x} Cs _x)Zn(SCN) ₄	Rb ⁺ , Cs ⁺	0 ≤ x ≤ 1	86
λ-(ET) ₂ (GaCl ₄) _{1-x} (CoCl ₄) _x	GaCl ₄ ⁻ , CoCl ₄ ²⁻	0 ≤ x ≤ 0.06	87
δ ⁺ -(ET) ₂ (GaCl ₄) _{1-x} (CoCl ₄) _x	GaCl ₄ ⁻ , CoCl ₄ ²⁻	0.05, 0.14	87
α-(ET) ₃ (CoCl ₄) _{1-x} (GaCl ₄) _x (TCE)	GaCl ₄ ⁻ , CoCl ₄ ²⁻	0.54, 0.57, 0.62	87
β ¹ -(ET) ₃ (CoCl ₄) _{1-x} (GaCl ₄) _x	GaCl ₄ ⁻ , CoCl ₄ ²⁻	0.88, 0.66	87
β ² -(ET) ₂ (SF ₅ RSO ₃) _{1-x} (SF ₅ R'SO ₃) _x	R, R' = CH ₂ CF ₂ , CHF	0 ≤ x ≤ 1	88
β ² -(ET) ₂ (SF ₅ RSO ₃) _{1-x} (SF ₅ R'SO ₃) _x	R,R' = CH ₂ -CF ₂ , CHF ₂	0 ≤ x ≤ 1	88
λ-(BETS) ₂ GaBr _x Cl _{4-x}	(GaBr _x Cl _{4-x}) ⁻ (x = 1-4)		89,90
λ-(BETS) ₂ GaF _x Cl _{4-x}	(GaF _x Cl _{4-x}) ⁻ (x = 1-4)		91
λ-(BETS) ₂ Fe _x Ga _{1-x} Cl ₄	FeCl ₄ ⁻ , GaCl ₄ ⁻	0.43, 0.55	92,93,94
(DIETSe) ₂ GaBr _x Cl _{4-x}	(GaBr _x Cl _{4-x}) ⁻ (x = 1-4)		95
(DIETSe) ₂ FeBr _x Cl _{4-x}	(FeBr _x Cl _{4-x}) ⁻ (x = 1-4)		95
(TTM-TTP)FeBr _x Cl _{4-x}	(FeBr _x Cl _{4-x}) ⁻ (x = 1-4)		96
(TTM-TTP)GaBr _x Cl _{4-x}	(GaBr _x Cl _{4-x}) ⁻ (x = 1-4)		97
(TTM-TTP)Fe _{1-x} Ga _x Cl ₄	FeCl ₄ ⁻ , GaCl ₄ ⁻	0.1	97

(TTM-TTP)Fe _{1-x} Co _x Cl ₄	FeCl ₄ ⁻ , CoCl ₄ ²⁻	0.05, 0.40	98
(TTM-TTP)Ga _{1-x} Co _x Cl ₄	GaCl ₄ ⁻ , CoCl ₄ ²⁻	0.30	98
(TTM-TTP)Mn _{1-x} Co _x Cl ₄	MnCl ₄ ²⁻ , CoCl ₄ ²⁻	0.90	98
β-(EDT-TTF-I ₂) ₂ [Pb _{2/3+x} Ag _{1/3-2x} □ _x I ₂] ₃	Pb ²⁺ , Ag ⁺	0.05	99

2. Chemical properties of solid solutions in molecular conductors

In the following, we will describe the different methods used for the elaboration of solid solutions of molecular conductors, together with the analytical methods used to particularly characterize their composition. We will also address important issues about the nature of the mixed species (volume, shape, charge, spin, etc).

2.1 Crystal growth methods

Crystalline molecular conductors are essentially obtained through two different methods involving both an electron transfer, either crystallization from solution using an oxidant or reducing agent (eventually inserted itself in the structure), and electrocrystallization where the electron transfer performed at the electrode is followed by the precipitation (crystallization) of the conducting salts on the electrode itself.

2.1.1 Cocrystallizations. This first approach is illustrated by the well-known TTF•TCNQ conductor. Its extension to solid solutions with the selenated analog, i.e. tetraselenafulvalene (TSF) has been reported already in 1977 for (TSF)_x(TTF)_{1-x}(TCNQ),³⁴ obtained either by slow diffusion of the constituents together³⁵ or by cooling from saturated solutions, with x varying continuously between 0 and 1. On the other hand, the solid solution (HMTTF)_x(HMTSF)_{1-x}•TCNQ could be prepared only with x = 0.05 for a nominal concentration in solution of x = 0.25, an indication of the probably much lower solubility of the selenated phase.³⁷

Reducing agents such as TDAE [tetrakis(dimethylamino)ethylene] are used for the elaboration of TDAE•(C₆₀)_{1-x}(C₇₀)_x alloys, which precipitate rapidly from solutions of C₆₀ and C₇₀ in a benzene/toluene mixture.⁶⁴ TDAE was also used a reducing agent without insertion in the crystal in the single-component conductor derived from the reduction of the spiro-bis(9-oxidophenalenone)boron cation noted [PLY(O,O)]₂B⁺.⁵³ Co-crystallization of solutions of spiro-bis(9-oxidophenalenone)boron cation [PLY(O,O)]₂B⁺ mixed with selected amounts of the neutral beryllium analog [PLY(O,O)]₂Be in the presence of TDAE leads to the formation of a series of solid-state solutions of composition [PLY-(O,O)]₂B_{1-x}Be_x. The crystallization

process is driven by the insolubility of radical $[\text{PLY}(\text{O},\text{O})]_2\text{B}$, which apparently induces the co-crystallization of $[\text{PLY}(\text{O},\text{O})]_2\text{Be}$ with x values not exceeding 0.2. Higher Be concentrations are reached in the methyl-substituted analogs with x values up to 0.59.⁵⁴

Reduction processes are also involved in the preparation of solid solutions of the DCNQI acceptor and analogs. As reported by Hünig *et al.*, mixing two (or even three) different DCNQI in the presence of CuBr_2 and a copper wire afforded crystallization of 26 binary and even one ternary alloys such as $[(\text{Me}_2)_{1-x}(\text{MeBr})_x\text{DCNQI}]_2\text{Cu}$.⁶¹ Under these conditions, the different reduction potentials of two DCNQI does not affect the composition of the salt and the most reducible acceptor was not inserted preferentially. Solid solutions involving Me_2DCNQI and for example its deuterated analog $\text{Me}_2\text{DCNQI-d}_8$ were also prepared upon reaction of the acceptor molecules with Bu_4NI as reductant in the presence of a copper salt, namely $(\text{Et}_4\text{N})_2\text{CuBr}_4$.⁵⁸ These DCNQI salts can be also prepared by electrocrystallization (see below).^{59,60}

Chemical oxidation processes have been also used in the crystallization of solid solutions of $[\text{Pd}(\text{dmit})_2]$ dithiolene complexes, such as $(\text{Me}_4\text{Sb})_{1-x}(\text{EtMe}_3\text{Sb})_x[\text{Pd}(\text{dmit})_2]_2$ or $(\text{Et}_2\text{Me}_2\text{Sb})_{1-x}(\text{EtMe}_3\text{Sb})_x[\text{Pd}(\text{dmit})_2]_2$.⁶⁷ They are prepared indeed through the slow air oxidation of $[\text{Pd}(\text{dmit})_2]^{2-}$ ion in the presence of the corresponding cations (Me_4Sb^+ vs. EtMe_3Sb^+ or $\text{Et}_2\text{Me}_2\text{Sb}^+$ vs. EtMe_3Sb^+) and acetic acid. This method proved very suitable for the preparation of large and high-quality alloyed crystals.

2.1.2. Electrocrystallizations. Electrocrystallization is by far the most general method used for the elaboration of molecular conductors.¹⁰⁰ The method for preparing solid solutions containing *two different electroactive species* (Table 1) is based on their mixing in the anodic (for donor molecules) or the cathodic (for acceptor molecules) compartment of the electrocrystallization cell, in the presence of the chosen electrolyte dissolved in both compartments. A constant current intensity is usually applied for several days/weeks. The main series of alloys explored so far are the Fabre/Bechgaard salts where mixing of TMTTF and TMTSF were performed in their 2:1 salts with ClO_4^- ,⁴⁰ ReO_4^- ,⁴¹ and PF_6^- .⁴³ Indeed both TMTTF and TMTSF salts exhibits closely related structures and can be described by a unique (p,T) phase diagram.¹⁸ Considering that both molecules do not oxidize at the same potential, the PF_6^- alloy $[(\text{TMTSF})_{1-x}(\text{TMTTF})_x]_2\text{PF}_6$ was originally prepared in a *potentiostatic* mode at 0.25-0.30 V, i.e. below the oxidation potential of both donor molecules (TMTTF: +0.26 V; TMTSF: +0.43 V).⁴³ A slightly different strategy was used for the ClO_4^- alloy prepared at a higher intermediate potential value (0.4 V).⁴⁰ The smaller solubility of the TMTSF salts limited

however the insertion of TMTTF to a maximum value of $x = 0.30$ in $[(\text{TMTSF})_{1-x}(\text{TMTTF})_x]_2\text{ClO}_4$, and of $x = 0.25$ in $[(\text{TMTSF})_{1-x}(\text{TMTTF})_x]_2\text{PF}_6$. These problems were not found for the ReO_4^- salt, i.e. $[(\text{TMTSF})_{1-x}(\text{TMTTF})_x]_2\text{ReO}_4$,⁴¹ where galvanostatic methods associated with smaller current densities and hence a slower crystallization process afforded three alloys with $x \approx 0.2, 0.55$ and 0.8 . The well-known κ -(ET)₂Cu[N(CN)₂]Br kappa-Br phase has been also the subject of alloying strategies involving as second donor molecules BEDT-STF or BEDSe-TTF.^{44,45} Finally, dithiolene complexes offer another series where solid solutions can be easily prepared by electrocrystallization of two different complexes differing only by the nature of the central metal, either in isoelectronic series such as Ni/Pd/Pt complexes or by modifying the overall electron count in Ni/Au, Pt/Au or Ni/Cu solid solutions.⁴⁷⁻⁵⁷

Electrocrystallization is the synthetic method of choice for the elaboration of solid solutions involving *two different counter-ions* of analogous symmetry, shape and charge, as for example ClO_4^- vs. ReO_4^- . Numerous examples have been reported and some are collected in Table 2. In most cases, the whole composition range can be explored. Also, because the electrolytes are used in large excess compared to the electroactive species, very small x values can be explored when doping effects are considered rather than exploration of the whole $0 \leq x \leq 1$ range. Electrocrystallization conditions might require a difficult optimization in order to be able to isolate solid solutions with a broad composition range. For example, in the series of β -(ET)₂(X1)_{1-x}(X2)_x alloys ($\text{X1}, \text{X2} = \text{I}_3^-, \text{I}_2\text{Br}^-, \text{IBr}_2^-$),⁷⁸ the mixed crystals having a wide composition of anions were obtained from only nitrobenzene for $\text{X1} = \text{IBr}_2^-$ and $\text{X2} = \text{I}_3^-$, from only chlorobenzene for $\text{X} = \text{I}_2\text{Br}^-$ and $\text{X2} = \text{I}_3^-$, and from only THF for $\text{X1} = \text{I}_2\text{Br}^-$ and $\text{X2} = \text{IBr}_2^-$ respectively, and the crystals having such a wide composition of anions were not obtained from other organic solvents. Note that the electrocrystallization itself can generate two different anions, as reported upon crystal growth of β -(BEDT-TTF)₂AuI₂ in the presence of solely Bu_4NAuI_2 . When performed at high potentials, it afforded the solid solution β -(BEDT-TTF)₂[(AuI₂)_{0.26}(I₃)_{0.74}], a probable consequence of the oxidation and decomposition of the AuI_2^- anion.⁸⁰

2.2 Nature of the components of a molecular alloy

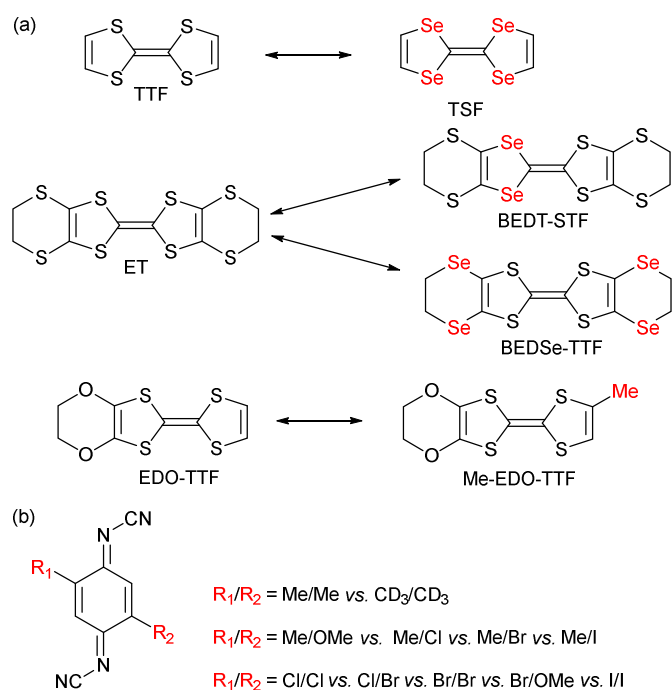
Engineering molecular solid solutions is not always a straightforward task.¹⁰¹ It is essentially based on the assumption that the similarity of size and shape is sufficient, albeit the intermolecular interactions between molecules in the crystal also play an important role.¹⁰² In

that respect, the examples reported in Tables 1 and 2 are not so numerous and often limited to very similar systems.

Perhaps the most identical, yet different molecules to be alloyed are those with *different isotopes* (H vs. D, ^{13}C , ^{34}S , ^{77}Se). In the field of molecular conductors, isotope introduction has been originally performed in order to observe any change in Tc, i.e. the "isotope effect" in superconducting salts.¹⁰³ Besides, solid state NMR is an important tool to investigate the magnetic and conducting properties of such systems in order to estimate the density of states from the Knight-shift and the spin–lattice relaxation rate. It requires a ^{13}C enrichment of the molecules, most often on the two central carbon atoms of the TMTTF,¹⁰⁴ TMTSF or BEDT-TTF molecules.¹⁰⁵ With this enrichment, spectral splitting occurs because of the resulting coupled spin system and induces a so-called Pake doublet.¹⁰⁶ To avoid this problem, ^{13}C -enriched TMTTF or ET molecules were prepared from a mixture of marked and unmarked dithiole precursors, affording a mixture with 10% ^{13}C -TMTTF in unmarked TMTTF,¹⁰⁴ or containing less than 7% $^{13}\text{C}=^{13}\text{C}$ double side-enriched ET in a major ^{13}C -single side-enriched ET molecule.¹⁰⁵ These mixtures were electro-crystallized to yield solid solutions composed of double side-, single side-enriched and non-enriched donor molecules.

Another series where isotopic substitution proved particularly adapted is based on the Me_2DCNQI acceptor, also known as its fully deuterated analog, $\text{Me}_2\text{DCNQI-d}_8$.⁵⁸ Indeed, the slightly smaller size of deuterium vs. hydrogen makes deuteration of molecules a very useful tool to tentatively parallel the effect of an external pressure, as also explored in this area with BEDT-TTF-d_8 .¹⁰⁷

As shown in Scheme 2a, the donor molecules used in alloys of cation radical salts are essentially based on a S/Se substitution, on the central TTF core as well as on side substituents. One single example involves the introduction of an extra methyl group in the $[(\text{EDO-TTF})_{1-x}(\text{MeEDO-TTF})_x]_2\text{PF}_6$ alloys but the whole composition range could not be prepared but only for $x < 0.6$ or $x > 0.9$.⁴⁶ A much broader choice was offered in the $(\text{DCNQI})_2\text{Cu}$ salts where many acceptors with different substituents in the 2 and 5 positions could be mixed (Scheme 2b).



Scheme 2 (a) Examples of pairs of donor molecules investigated in alloys. (b) The different DCNQI acceptor molecules used in alloys.

Most common solid solutions involve *two different counter-ions* of analogous symmetry, shape and charge, as for example Cl^- vs. Br^- vs. I^- , ClO_4^- vs. ReO_4^- , PF_6^- vs. AsF_6^- vs. SbF_6^- , FeCl_4^- vs. GaCl_4^- , I_3^- vs. I_2Br^- vs. IBr_2^- , or in radical anion salts, Li^+ vs. Cu^+ , all collected in Table 2. In most cases, the whole composition range can be explored.

Organic counter-ions offer an increased degree of complexity as reported in the alloys involving Me_4Sb^+ vs. EtMe_3Sb^+ ,⁶⁷ or $\text{SF}_5\text{CH}_2\text{CF}_2\text{SO}_3^-$ vs. $\text{SF}_5\text{CHF}_2\text{SO}_3^-$.⁸⁸ In these salts, to the positional disorder of the two species on a given crystallographic site for the counter-ion is added a substitutional disorder even more difficult to characterize (see below section 2.4). A specific warning should be made here for reported solid solutions involving the pairs $\text{GaCl}_4^-/\text{GaBr}_4^-$, or $\text{FeCl}_4^-/\text{FeBr}_4^-$. Indeed, several interesting phases with the BETS donor molecule have been reported, such as the organic superconductor λ -(BETS)₂GaCl₄ or the isostructural λ -(BETS)₂FeCl₄ which exhibits a sharp MI transition around 8 K. On the other hand, κ -type salts with various anions such as GaCl_4^- , GaBr_4^- , FeCl_4^- , FeBr_4^- , and InCl_4^- exhibit metallic behavior down to 4 K.²⁴ Solid solutions of the λ -phases were investigated with for example GaCl_4^- and GaBr_4^- in a 1:3 ratio written as " GaBrCl_3^- ".^{89,90} It has been reported however that the halogen ions of mixed halide gallium anions tend to be easily substituted by another halogen ions in solution.¹⁰⁸ This scrambling in solution implies that the description " GaBrCl_3^- " does not represent just one species GaBrCl_3^- , but rather the complex mixture of

GaCl_4^- , GaBrCl_3^- , $\text{GaBr}_2\text{Cl}_2^-$, GaBr_3Cl^- , and GaBr_4^- . In the present example, the distribution was approximatively 5:6:3:1:0 and the Br/Cl distribution was different on the four crystallographically different halide sites. Similar scrambling reactions and added complexity are also reported in solid solution involving the DIETS or TTM-TTP donor molecules with the iron complexes $\text{FeCl}_4^-/\text{FeBr}_4^-$.^{95,96}

2.3 Miscibility: doping, preferential insertion

In several situations where the two extreme structures differ too much from each other, a full miscibility of the two partners cannot be reached and the resulting salts are much better described as doped materials. These compositions are also of interest for highly sensitive properties such as superconductivity (see below in Section 3), upon insertion of disorder or of magnetic defects. For example, insertion of the tetrahedral and magnetic ($S = 5/2$) FeCl_4^- anion into $(\text{TMTSF})_2(\text{AsF}_6)$ was limited to a x value of 10^{-3} in the alloy formulated as $(\text{TMTSF})_2(\text{AsF}_6)_{1-x}(\text{FeCl}_4)_x$, despite a 8:2 ratio $\text{AsF}_6^-:\text{FeCl}_4^-$ in the electrolyte.⁷³ Such doped systems are also prepared on purpose for EPR investigations of paramagnetic dithiolene complexes diluted in diamagnetic matrices, as for example $[\text{Ni}(\text{dt})_2]^-$ in diamagnetic $[\text{Au}(\text{dt})_2]^-$,¹⁰⁹ or $[\text{Cu}(\text{dt})_2]^{2-}$ in diamagnetic $[\text{Ni}(\text{dt})_2]^{2-}$.¹¹⁰

In most situations however, the full range of compositions can be obtained but often with a x value in the crystal which differs from the nominal concentration in solution. Concerning the S/Se exchange in donor molecules, $(\text{TSF})_x(\text{TTF})_{1-x}(\text{TCNQ})$ is the only example where a slight enrichment in TTF is observed over that of the initial solution composition.³⁴ Other examples go in the opposite direction, *i.e.* a systematic preferential insertion of the selenated molecule associated with a decreased solubility of the corresponding salt, as in $[(\text{TMTSF})_{1-x}(\text{TMTTF})_x]_2\text{ClO}_4$,^{40a} $[(\text{TMTSF})_{1-x}(\text{TMTTF})_x]_2\text{PF}_6$,⁴³ $(\text{HMTTF})_{0.05}(\text{HMTSF})_{0.95}\text{TCNQ}$,³⁷ or $\kappa\text{-}[(\text{ET})_{1-x}(\text{BEDSeT-TTF})_x]_2\text{Cu}[\text{N}(\text{CN})_2]\text{Br}$.⁴⁵ Similar strong effects are observed within radical-anion salts as the DCNQI alloys $[(\text{Me}_2)_{1-x}(\text{MeBr})_x\text{DCNQI}]_2\text{Cu}$, where a 0.2 molar fraction of $(\text{MeBr})\text{DCNQI}$ in solution results in a $x = 0.7$ fraction in the solid.^{59,60} Systematic studies related to these preferential insertion effects are scarce but give an invaluable information about the relative stability/solubility of two different compounds differing only by the counterion. In that respect we can mention for example the mixed-valence 1:2 salts of the electroactive $[\text{Pd}(\text{dmit})_2]$ with either Me_4Sb^+ , EtMe_3Sb^+ and $\text{Et}_2\text{Me}_2\text{Sb}^+$ cations.⁶⁷ As shown in Fig. 1, the molar fraction of the bulkier/disordered EtMe_3Sb^+ cation in crystalline solid solutions with Me_4Sb^+ is systematically smaller than in the electro-crystallized solution, showing a more “favorable” crystal growth with the more compact Me_4Sb^+ cation. On the other hand,

introduction of the even bulkier $\text{Et}_2\text{Me}_2\text{Sb}^+$ cation in competition with EtMe_3Sb^+ (Fig. 1b) gives no sign for discrimination, a consequence of the similar steric constraints brought by the two ethyl-containing cations. Indeed, in the pristine EtMe_3Sb^+ salt, the EtMe_3Sb^+ cation is located on a two-fold axis and exhibits a disorder with two possible orientations, giving an overlapped image with an apparent $\text{Et}_2\text{Me}_2\text{Sb}^+$ cation with 50% occupancy of the ethyl groups.

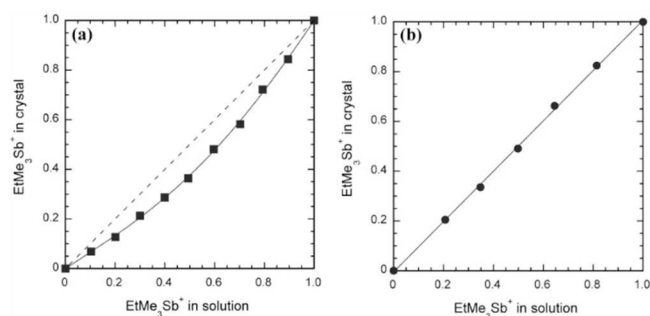


Fig. 1 Mole fraction of EtMe_3Sb^+ in the crystal (x) as a function of that in solution for (a) $(\text{Me}_4\text{Sb})_{1-x}(\text{EtMe}_3\text{Sb})_x[\text{Pd}(\text{dmit})_2]_2$ and (b) $(\text{Et}_2\text{Me}_2\text{Sb})_{1-x}(\text{EtMe}_3\text{Sb})_x[\text{Pd}(\text{dmit})_2]_2$. Reproduced from Ref 67 with authorization of Wiley-VCH.

A very different situation is observed in 2:1 cation radical salts of *o*- Me_2TTF with the Cl^- , Br^- and I^- anions.⁶⁸ In this original quadratic structure, the halide is embedded in a set of weak $\text{C}-\text{H}\cdots\text{X}^-$ hydrogen bonds. Solid solutions were reported involving either Cl^-/Br^- , or Br^-/I^- pairs. As shown in Fig. 2, preferential insertion is observed here with the Br^- anion, in solid solutions with either Cl^- or I^- , demonstrating that the most “stable” structure, or the best compromise between size and all intermolecular interactions is reached with the intermediate-size Br^- anion. Note that the authors reported that this bromide phase actually gives the largest crystals during the electrocrystallization experiments.

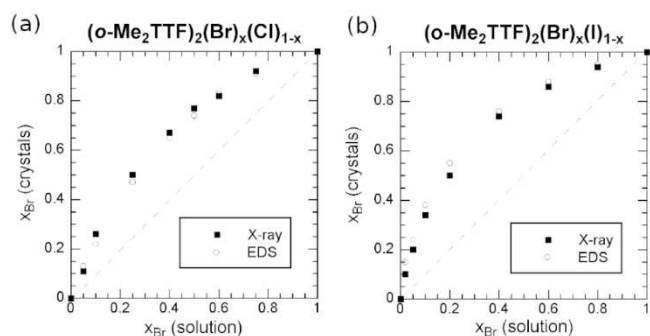


Fig. 2 Mole fraction (x) of the Br^- anion in the crystals, as a function of that in solution for (a) $(o\text{-Me}_2\text{TTF})_2(\text{Br})_x(\text{Cl})_{1-x}$ and (b) $(o\text{-Me}_2\text{TTF})_2(\text{Br})_x(\text{I})_{1-x}$. Reproduced from Ref. 68 with authorization of Wiley-VCH.

More complex anions can also give similar effects as reported in $\theta\text{-(BEDT-TTF)}_2(\text{Rb}_{1-x}\text{Cs}_x)\text{Zn}(\text{SCN})_4$ with preferential insertion of Cs^+ over Rb^+ ,⁸⁶ or in $\kappa\text{-(BEDT-TTF)}_2\text{Cu}[\text{N}(\text{CN})_2]\text{Br}_x\text{Cl}_{1-x}$ salts with preferential insertion of the Br^- ion.⁸³

2.4 Disorder evaluation

In essentially all reported examples, the statistical mixing of two partners in the solid solution is taken for granted. This point was investigated on one single example by X-ray diffraction at low temperatures ($T < 30$ K) where the diffuse scattering due to thermal vibrations is negligible, in comparison with the effects of an intrinsic substitutional disorder. In $\text{TMTSF}_2(\text{ReO}_4)_{1-x}(\text{ClO}_4)_x$ solid solutions,⁷¹ the intense diffuse scattering observed near the origin of the reciprocal space was shown to decrease with increasing Bragg (θ) angle. This θ dependence follows, at all concentrations, the monotonic Laue scattering associated with random disorder which writes as:

$$I(\theta) = Cx(1-x)[f_A(\theta) - f_B(\theta)]^2$$

where f_A and f_B are the form factors of the ReO_4^- and ClO_4^- anions and C a scale factor. Since (i) the anions orientation is similar in both pure salts and (ii) the Re-O and Cl-O distances are also comparable, it was confidently concluded that the $\text{ReO}_4^-/\text{ClO}_4^-$ substitutional disorder is indeed random for all concentrations in this salt.

The question of substitutional vs. positional disorder was elegantly addressed in the $\beta''\text{-(BEDT-TTF)}_2(\text{SF}_5\text{-R-SO}_3)$ series known to exhibit superconducting ($\text{R} = \text{CH}_2\text{CF}_2$), metallic ($\text{R} = \text{CHF}$), or metal-insulator ($\text{R} = \text{CHF}\text{CF}_2$) character.⁸⁸ With the latter chiral $\text{SF}_5\text{CHF}\text{CF}_2\text{SO}_3^-$ anion, a positional disorder of the two enantiomers is observed in the pure phase and two characteristic, low-energy electronic excitations (centered at ≈ 5200 and 9600 cm^{-1}) were tentatively attributed to either correlation-driven or disorder-related localization. To test this assumption, solid solutions were prepared. When associating the superconducting ($\text{R} = \text{CH}_2\text{CF}_2$) and metallic ($\text{R} = \text{CHF}$) systems, only positional disorder is expected. The strongest charge-transfer excitations are observed for $x = 0.5$ where positional disorder is indeed maximum. On the other hand, when associating the superconducting ($\text{R} = \text{CH}_2\text{CF}_2$), with the metal-insulator ($\text{R} = \text{CHF}\text{CF}_2$) chiral anion, it appears that local orientational disorder effects

(chiral anion) are much stronger than positional effects (alloying) as the strongest charge-transfer excitations are observed for $x = 1$. It demonstrates that the anion pocket disorder results in large-amplitude modulations of the electrostatic potential, which are very effective in localizing charge on the BEDT-TTF stack, revealed by these low-energy electronic excitations.

A specific situation needs to be mentioned where order emerges from disorder for 50:50 composition, for example in the $[(\text{TMTSF})_{1-x}(\text{TMTTF})_x]_2\text{ReO}_4$ for $x \approx 0.50$.⁴¹ Independently of the $q_1 = (\frac{1}{2}, \frac{1}{2}, \frac{1}{2})$ surstructure associated with well-known anion ordering (AO) transition observed at low temperatures in both pure compounds and the alloys, another $q_2 = (0, \frac{1}{2}, \frac{1}{2})$ surstructure found already at room temperature has been attributed to an alternate order of the TMTTF and TMTSF molecules along the stacks, with a spatial coherence of $\approx 300 \text{ \AA}$.

2.5 Tools to analyze solid solution's composition

The evaluation of the exact composition and nature of solid solutions is a complex challenge. Several points are indeed of interest for any analytical method aimed at determining the alloy composition, such as its precision (important for low x values), its spatial extension, its reproducibility also in relation with the homogeneity of the samples themselves, and its eventual destructive character.

Energy-dispersive X-ray spectroscopy (EDS, EDX, EDXS or XEDS), sometimes called energy dispersive X-ray analysis (EDXA or EDAX) or energy dispersive X-ray microanalysis (EDXMA), is the analytical technique of choice to analyze most solid solutions. Different elements can be probed simultaneously, as for example S vs. Se in $(\text{TSF})_x(\text{TTF})_{1-x}(\text{TCNQ})$,³⁴ $[(\text{TMTSF})_{1-x}(\text{TMTTF})_x]_2\text{PF}_6$,⁴³ or $\kappa\text{-}[(\text{ET})_{1-x}(\text{BEDSeT-TTF})_x]_2\text{Cu}[\text{N}(\text{CN})_2]\text{Br}$.⁴⁵

X-ray diffraction on single crystals is a useful tool when the two mixed species differs notably by their electron count and hence their diffracting power. Typical examples involve refinement of Cl^- vs. Br^- in $(o\text{-Me}_2\text{TTF})_2\text{Cl}_{1-x}\text{Br}_x$,⁶⁸ of Br vs. CH_3 in $[(\text{Me}_2)_{1-x}(\text{MeBr})_x\text{DCNQI}]_2\text{Cu}$,⁶⁰ of Ni vs. Pd in $[(\text{CH}_3)_4\text{N}][\text{Ni}_x\text{Pd}_{1-x}(\text{dmit})_2]_2$,⁵⁷ of Pt vs. Au in $(\text{Perylene})_2[\text{Au}_{1-x}\text{Pt}_x(\text{mnt})_2]$.⁴⁹ The method however requires that a complete data set is collected and refined for each composition while EDS methods (see above) provide comparable precision in a much faster way. On the other hand, the method gives a precise indication on the evolution of the structure (unit cell, molecular orientations) with x .

Inductively Coupled Plasma – Atomic Emission Spectroscopy (ICP-AES) has been used only rarely and is mentioned to evaluate the beryllium amount in the $[\text{PLY}-(\text{O},\text{O})]_2\text{B}_{1-x}\text{Be}_x$

solid solutions of spiro-bis(9-oxidophenalenone)boron [PLY(O,O)]₂B with the neutral beryllium analog [PLY(O,O)]₂Be.^{53,54}

Neutron activation analysis (NAA) has been reported by two groups to analyze solid solutions, in mixed crystals of (BEDT-TTF)-trihalides such as β -(ET)₂(I₃)_{1-x}(IBr₂)_x, β -(ET)₂(IBr₂)_{1-x}(I₂Br)_x and β -(ET)₂(I₂Br)_{1-x}(I₃)_x to determine the atomic ratio of bromine and iodine,^{77,78} and in the extensive series of (DCNQI)₂Cu salts to analyze Br and Cu.⁶¹

Elemental analysis can be used but its precision is relatively low, it requires large amounts of materials, most often not available when obtained by electrocrystallization. The method has therefore been limited to materials obtained in larger quantities by chemical routes, as in the series of (DCNQI)₂Cu salts,⁶¹ or in magnetic salts such as [NO₂BzPy][Au_xNi_{1-x}(mnt)₂] where [NO₂BzPy]⁺ stands for 1-(4'-nitrobenzyl)pyridinium and [M(mnt)₂]⁻ for bis(maleonitriledithiolato)metallate.^{55,56}

Mass spectrometry (EI-MS) has been used to discriminate between closely related molecular species, as between EDO-TTF and MeEDO-TTF in [(EDO-TTF)_{1-x}(MeEDO-TTF)_x]₂PF₆, where the two molecules only differ by a methyl group.⁴⁶ Experimental deviations of the x value were \approx 0.01-0.02. It should be noted that the estimation of x values in this method should bear some systematic error since efficiencies of EDO-TTF and MeEDO-TTF molecules to produce molecular ions should be different from each other. The same method was used for the mixed-valence [Pd(dmit)₂] salts with mixtures of Me₄Sb⁺, EtMe₃Sb⁺ or Et₂Me₂Sb⁺ cations.⁶⁷

Solution NMR has been reported on one recent example for (TMTSF)₂(TaF₆)_{1-x}(PF₆)_x solid solutions involving TaF₆⁻ and AsF₆⁻ anions thanks to ¹⁹F NMR measurements of solutions prepared by dissolving small amounts of each material in DMSO-d₆.⁷⁶ The integration of the signal of PF₆⁻, appearing as a doublet at -70 ppm with respect to the signals of fluorine atoms connected to Ta(V) provided the ratio TaF₆⁻/PF₆⁻ in the bulk material. Satisfyingly, the ratios estimated by this method were in good agreement with those obtained by the refinement of the single crystal diffraction data.

3. Manipulation of physical properties in solid solutions

Investigations of solid solutions in molecular conductors are associated with a variety of objectives, which concern the analogy with external pressure effects (chemical pressure), the influence of disorder and/or doping on conductivity and eventually superconductivity, the manipulation of band filling, the insertion of magnetic defaults, the evolution of structural

and/or electronic phase transitions characteristics of the pure compounds. These effects proved to be very complex to analyze and they will be illustrated in the following by only some representative examples.

3.1 Chemical pressure effects

Once the actual composition of the solid solution (x value in crystal) has been determined (Cf above Section 2.6), it is possible to follow the evolution of the unit cell parameters with x . In the only situations where both pure compounds have the same crystal structure, a linear evolution of these parameters between the $x = 0$ and the $x = 1$ situations is often observed, referred as the Vegard's law. Typical examples are reported for example in $(\text{TMTSF})_2(\text{ClO}_4)_{1-x}(\text{ReO}_4)_x$,⁷¹ θ - $(\text{BEDT-TTF})_2(\text{Rb}_{1-x}\text{Cs}_x)\text{Zn}(\text{SCN})_4$,⁸⁶ $(o\text{-DMTTF})_2\text{Br}_x\text{Cl}_{1-x}$,⁶⁸ or β - $(\text{BEDT-TTF})_2(\text{I}_3)_{1-x}(\text{IBr}_2)_x$.^{77,78} These linear evolutions are often described, in a misuse of language, as chemical pressure effects, as in most cases the actual evolutions of the pure systems under pressure are not known. In other words, the compressibility (and its anisotropy) of a pure system might be notably different from its evolution in a solid solution upon insertion of a smaller species. An illustration is provided by the β - $(\text{ET})_2(\text{I}_3)_{1-x}(\text{IBr}_2)_x$ alloy where the smooth evolution of the unit cell parameters (contraction with increasing amounts of the smaller IBr_2^- anion) parallels that observed in the pure β - $(\text{ET})_2\text{I}_3$ phase ($x = 0$) under pressure between 0 and 4 kbar. The pure IBr_2^- phase ($x = 1$) is indeed crystallographically comparable to that of the $x = 0$ I_3^- phase at 4 kbar.⁷⁷ The situation is more delicate in the κ - $(\text{BEDT-TTF})_2\text{Cu}[\text{N}(\text{CN})_2]\text{Br}_x\text{Cl}_{1-x}$ system^{83,85} where increasing amounts of Br^- anions do play the same effect than that of the physical pressure on the pure chloride salts ($x = 0$) while the unit cell volume is actually increasing (negative chemical pressure) with x .

Deviations from Vegard's law are common and can be indicative of evolution of the molecular orientations such as tilt angle of the stacks in $(\text{TSeF})_x(\text{TTF})_{1-x}\cdot\text{TCNQ}$.³⁴ Such displacements are characteristic of molecular alloys and can have important consequences on the physical properties up to the point where a continuous change of composition can have non-linear effects on the structural and hence electronic properties. This point is beautifully illustrated in the behavior of solid solutions of the $(\text{DCNQI})_2\text{Cu}$ salts. Indeed, two groups emerge from this family, those with a stable metallic state down to low temperatures with Me_2DCNQI or I_2DCNQI , and those with a sharp metal-insulator transition as found with $\text{Me}_2\text{DCNDI-d}_8$, MeBrDCNQI or MeClDCNQI .⁵⁸⁻⁶¹ The first group is sensitive to pressure and undergoes a metal-insulator transition, at a very low pressure (≈ 50 bar) in $(\text{Me}_2\text{DCNQI})_2\text{Cu}$ but

a notably higher one (15.3 kbar) in the I_2 DCNQI salt, indicating a very stable metallic state in the latter. Solid solutions associating two acceptors from group I, or two acceptors from group II, led to the expected group I or group II behavior respectively.^{61,62} On the other hand, associating two acceptor molecules, one from each group, into solid solutions was reported for example in $[(Me_2)_{1-x}(MeBr)_xDCNQI]_2Cu$, where small doping range ($x < 0.1$) was already sufficient to favor the apparition of the M-I transition, with re-entrance of the metallic phase at lower temperatures. This behavior was already known for the pristine $(Me_2DCNQI)_2Cu$ under pressure.⁵⁹ The main origin of these evolutions is however to be found in the evolution of the structure itself, with the α angle characterizing the tetrahedral coordination around the Cu ion which exhibits a notable increase with MeBrDCNQI concentration (Fig. 3).⁵⁹ This sensitivity varies with the nature of the acceptors. In the alloy $[(MeIDCNQI)_{1-x}(MeBrDCNQI)_x]_2Cu$, the group I behavior of $(MeIDCNQI)_2Cu$ was for example maintained up to $x = 0.60$.⁶¹ These examples illustrate how prudent one should be when referring to chemical pressure effects.

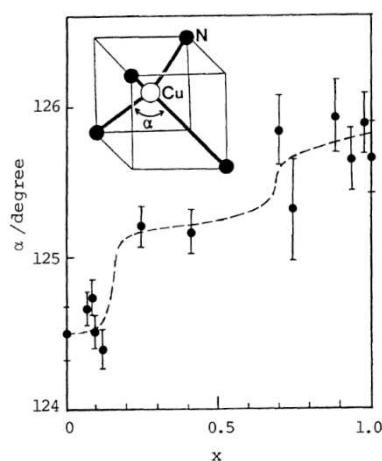


Fig. 3 Evolution of the α angle with x in the coordination sphere of Cu in the $[(Me_2)_{1-x}(MeBr)_xDCNQI]_2Cu$ alloys. Taken from ref 59 ©1989 The Chemical Society of Japan.

Another convincing illustration is provided by the $[(Me_2DCNQI)_{1-x}(Me_2DCNQI-d_8)_x]_2Cu$ alloys involving the deuterated $Me_2DCNQI-d_8$ belonging to group II. This system clearly reproduced the low-pressure region (1-500 bar) of the exotic pressure-temperature phase diagram of $[Me_2DCNQI]_2Cu$ including the reentrant M-I-M transition at ambient pressure.⁵⁸ The sharp transitions observed in the resistivity measurements indicated that the system is homogeneous and that the disorder effect brought by deuteration was reduced here to a minimum, which cannot be realized in other alloyed $(DCNQI)_2Cu$ salts. In this case, the very high sensitivity of the $[Me_2DCNQI]_2Cu$ system against pressure and the chemical pressure

control using the deuteration were the key elements for reproducing with alloying the pressure-temperature diagram of the pure hydrogenated system.

3.2 Anion ordering transitions

Since the TMTTF/TMTSF (Fabre/Bechgaard) salts crystallize in the $P\bar{1}$ space group with the counter ion located on inversion center, non-centrosymmetric anions such as ReO_4^- or ClO_4^- are disordered at room temperature. At low temperatures, they order in such a way that neighboring anions align or alternate their orientation. In $(\text{TMTSF})_2\text{ReO}_4$, the anions alternate in the three crystallographic directions below $T_{\text{AO}} = 176$ K, an ordering characterized by a reduced wave vector $q_1 = (\frac{1}{2}, \frac{1}{2}, \frac{1}{2})$. In $(\text{TMTSF})_2\text{ClO}_4$, the AO is found at $q_2 = (0, \frac{1}{2}, 0)$ with a much lower T_{AO} value (24 K), indicating an average decrease of the electron-anion coupling, the ClO_4^- anions having weaker interactions with the TMTSF stacks than the ReO_4^- ones.⁷⁰ In $(\text{TMTSF})_2(\text{ReO}_4)_{1-x}(\text{ClO}_4)_x$ solid solutions,⁷¹ it was shown that the q_1 long range order (LRO) of the ReO_4^- phase ($x = 0$) was kept for $x < 0.5$ while the q_2 LRO of the ClO_4^- phase ($x = 1$) was destroyed already for $x < 0.97$, with in-between, complex coexistence of short range order (SRO) at q_1 and q_2 . The phase diagram of this solid solution was analyzed within the framework of an Ising model, with an Ising variable $\eta_i = \pm 1$ depending on the anion orientation.

3.3 Alloying effects on conductivity

Conductivity of solid solutions is almost systematically investigated but its evolution with alloy composition and with temperature can be extremely complex to analyze as it depends on many different factors. We need for example to distinguish here two situations, those related to weak doping with x values close to 0 or 1, and those related to systems where x continuously covers the whole spectrum between 0 and 1. We will concentrate here on the second situation, and illustrate it first with the prototypical TTF•TCNQ system and its solid solution with TSF. As shown in Fig. 4, RT conductivity is decreased in the solid solution by comparison with the pure salts, a consequence of disordering the donor stack. This effect of disorder due to alloy formation also manifests itself in a smaller increase in conductivity with decreasing temperature. The conductivity increases indeed for the solid solutions by factors of 7-10 times in going from room temperature to the temperature T_{MI} at which it peaks (Peierls transition), compared to values for TTF•TCNQ and TSF•TCNQ of 12-20 times. Furthermore, the dominance of the TCNQ stacks and the unimportance of fulvalene disorder in producing the metal-insulator transition are confirmed for $0 < x < 0.9$,³⁶ as only 3% incorporation of TSF into TTF-TCNQ completely obscures the 38 K transition associated with the fulvalene stacks in

TTF-TCNQ, while the 53 K transition remains relatively sharp.³⁴ These evolutions are compared with those observed in an analogous salt isolated with the $(Z,E\text{-DTDSF})\cdot\text{TCNQ}$ (see Fig. 4). The notably higher RT conductivity of $(Z,E\text{-DTDSF})\cdot\text{TCNQ}$ when compared to that of the 50:50 solid solution indicates that the donor stack conductivity is much less affected by disorder due to the random arrangement of Z - and E - DTDSF molecules than that of the TSF and TTF molecules. This is because both Z - and E -DTDSF molecules are electronically very close, at variance with TSF and TTF whose oxidation potential differs by 0.17 V.³⁶

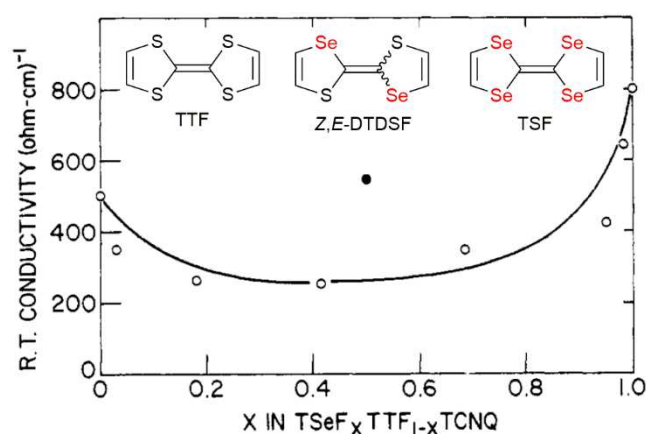


Fig. 4 Room temperature conductivity of $(\text{TSF})_x(\text{TTF})_{1-x}(\text{TCNQ})$ (open points). The closed black point refers to $[(Z,E)\text{-DTDSF}]\text{TCNQ}$ (see text). Adapted from ref. 34. © 1977 American Chemical Society.

Another example of the effect of disorder on the phase diagram is provided by the $(\text{TMTTF})_2(\text{SbF}_6)_{1-x}(\text{AsF}_6)_x$ solid solution. At low temperatures, a non-magnetic (Spin-Peirls) ground state is reported for $(\text{TMTTF})_2\text{AsF}_6$ while an antiferromagnetic ground state characterizes the pure SbF_6^- salt. The $(\text{TMTTF})_2(\text{SbF}_6)_{1-x}(\text{AsF}_6)_x$ alloys behave as the pure salts for $x < 0.2$ or $x > 0.8$, while in the middle range, higher disorder prevents the condensation of any ordered phase.⁷⁴

3.4 Alloying effects on superconductivity

The well-known sensitivity of superconductivity to disorder or defaults was investigated soon after it was discovered at ambient pressure in $(\text{TMTSF})_2\text{ClO}_4$. It was shown indeed that introduction of only 5% TMTTF in $[(\text{TMTSF})_{1-x}(\text{TMTTF})_x]_2\text{ClO}_4$, was sufficient to suppress superconductivity.⁴⁰ On the other hand, when replacing the ClO_4^- anion with a nominal

concentration of ReO_4^- up to $x = 0.06$ in $(\text{TMTSF})_2(\text{ClO}_4)_{1-x}(\text{ReO}_4)_x$, the superconducting transition temperature is depressed by a factor about two.^{72a,b}

β -(BEDT-TTF)₂I₃ is the first superconductor in the I₃⁻ salts of BEDT-TTF and was intensively studied at an early stage.²³ Coexistence of the high-T_c and low-T_c states was a puzzle that is related to an incommensurate lattice modulation below 200 K. In order to clarify this problem, an alloy system with the superconducting β -(BEDT-TTF)₂AuI₂ salt, β -(ET)₂(I₃)_{1-x}(AuI₂)_x, ($x = 0.1, 0.9$) was examined by low-temperature X-ray diffraction and transport measurements.^{79,81} It was suggested that two types of disorder, namely the conformational disorder of the terminal ethylene groups and the distortions in the anion sites, can affect the superconducting state. Superconductivity was destroyed in the $x = 0.1$ and $x = 0.6$ alloys while in the AuI₂⁻ rich phase ($x = 0.9$), stepwise resistivity drops were observed at 4.5 and 2.1 K. The high-temperature anomaly at 4.5 K has been associated to the high-T_c anomaly of β -(BEDT-TTF)₂I₃ and the superconducting transition at 2.1 K will correspond to the low-T_c transition.

In β -(BEDT-TTF)₂(I₃)_{1-x}(IBr₂)_x alloys, the superconductivity of the pure I₃⁻ phase was destroyed already for $x = 0.05$ and above while on the other side of the alloy, the superconducting state of the pure IBr₂⁻ phase was maintained for $x \geq 0.75$.⁷⁷ In that respect, the superconductivity of the so-called κ -Br phase of BEDT-TTF, i.e. κ -(BEDT-TTF)₂Cu[N(CN)₂]Br appears particularly robust as substitution of the donor molecule with the diselenated BEDT-SFT analog (see Scheme 2) allowed to maintain superconductivity for x values up to 0.20 in κ -[(BEDT-TTF)_{1-x}(BEDT-STF)_x]₂Cu[N(CN)₂]Br.⁴⁴

Similar disorder/size effects on superconductivity have been reported in the superconducting K₃C₆₀. The superconducting temperature of the pure compound K₃C₆₀ at 19K was progressively reduced upon alloying with C₇₀ in K₃(C₆₀)_{1-x}(C₇₀)_x and the SC state disappeared for $x > 0.25$.⁶³

3.5 Band filling manipulation

At variance with inorganic (super)conductors where band filling can be easily modified, for example through oxygen doping in high-T_c superconductors, molecular conductors with their fixed stoichiometry are most often not amenable to such strategies. Attempts have been reported however, (i) in cation-radical salts upon replacement of a monovalent anion by a divalent one ($\text{GaCl}_4^-/\text{FeCl}_4^-$ vs. $\text{MnCl}_4^{2-}/\text{CoCl}_4^{2-}$),^{87,98,111} (ii) in anion radical salts upon

replacement of $\text{Cu}^+/\text{Cu}^{2+}$ by Li^+ or (iii) in single component conductors where neutral metallic complexes are mixed with analogous neutral complexes having a different electron count.

Modification of band filling in cation radical salts proved very difficult as most often, the structure resists to the insertion of a divalent anion in place of a monovalent one. This strategy was successfully investigated for example in BEDT-TTF salts such as λ -(ET)₂(GaCl_4)_{1-x}(CoCl_4)_x with $x < 0.06$ or in δ' -(ET)₂(GaCl_4)_{1-x}(CoCl_4)_x with $x < 0.14$. In both systems, at maximum doping, the RT conductivity was found to decrease by one order of magnitude relative to the pure GaCl_4^- salts.⁸⁷ The most successful examples were reported from TTM-TTP salts, which are known to crystallize with monovalent anions (FeCl_4^- , GaCl_4^-) to give 1:1 phases, i.e. with a $\rho = 1$ charge transfer and associated $\frac{1}{2}$ band filling and a metallic character at RT, but also with divalent anions (MnCl_4^{2-} , CoCl_4^{2-}) with the same 1:1 stoichiometry and regular stacking but now with $\rho = 2$, zero band-filling and semiconducting character.⁹⁸ Three alloys were reported, associating CoCl_4^{2-} with either FeCl_4^- or GaCl_4^- in (TTM-TTP) $\text{Fe}_{1-x}\text{Co}_x\text{Cl}_4$ ($x = 0.05, 0.40$) and (TTM-TTP) $\text{Ga}_{1-x}\text{Co}_x\text{Cl}_4$ ($x = 0.30$). The decreased band filling associated with increasing x values was correlated with a regular increase of the room-temperature resistivity and thermoelectric power.

In radical anion salts, the $\text{Cu}(\text{DCNQI})_2$ system provides also a beautiful example of variable doping in the solid solutions where the copper is substituted by Li^+ . Indeed, in the pure $\text{Cu}(\text{DCNQI})_2$ salt, the valence of the copper is intermediate (+1.3) between that of Cu^+ and Cu^{2+} . Replacing progressively copper by Li^+ hence modifies continuously the band filling and turn the metallic $\text{Cu}(\text{DCNQI})_2$ system into a semiconductor in the whole temperature range (Fig. 5).^{65,66}

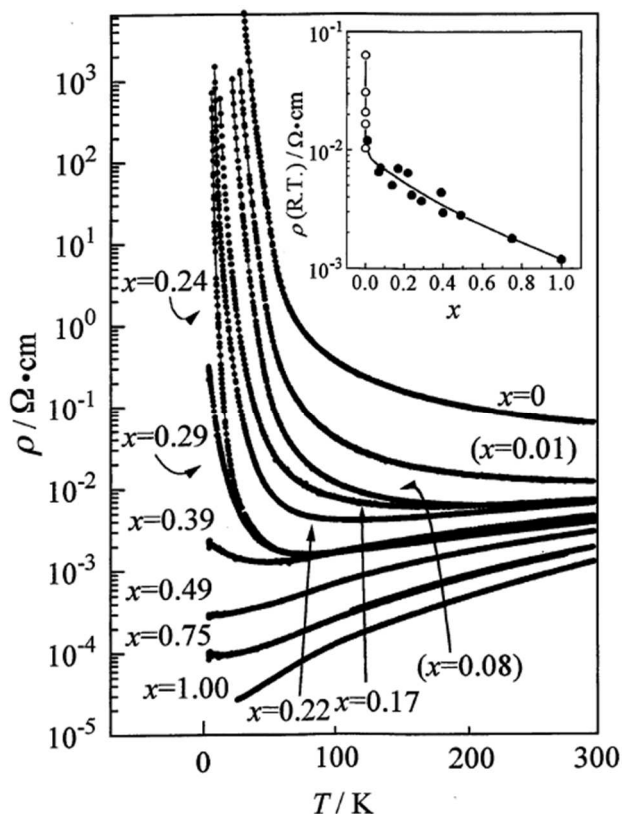


Figure 5 Temperature dependence of the resistivity of $(\text{DMDCNQI})_2\text{Li}_{1-x}\text{Cu}_x$. The insert shows the dependence of resistivity at RT with the white-centred for the $x = 0$ compound with various impurity levels. Reproduced from ref. 66. © 1999 The Physical Society of Japan.

Single-component conductors offer another playground for modifying the band filling, as illustrated below in several examples where neutral complexes of different electron count can be mixed. For example, $[\text{Ni}(\text{tmdt})_2]$ (see Scheme 1) is a 3D metal stable down to 4 K while $[\text{Au}(\text{tmdt})_2]$, bearing one extra electron, is reported to undergo an antiferromagnetic transition around 110 K (T_{Neel}) without loss of its high conductivity. The temperature dependence of the resistivities of the compressed pellet samples of the $[\text{Ni}_{1-x}\text{Au}_x(\text{tmdt})_2]$ alloys⁵¹ ($0 < x < 1$) showed the systems to be essentially metallic down to low temperature while T_{Neel} was moved to lower temperatures with decreasing x values, essentially disappearing for $x \leq 0.6$. Moving to solid solutions involving the isoelectronic copper analog $[\text{Cu}(\text{tmdt})_2]$ rather than the gold one gives a fully different picture,⁵² as the extra electron in $[\text{Cu}(\text{tmdt})_2]$ is now localized in an antibonding metal-ligand orbital of dx^2-y^2 symmetry. The magnetic behavior of $[\text{Ni}_{1-x}\text{Cu}_x(\text{tmdt})_2]$ for $x = 0.098, 0.13$ and 0.18 was described as a molecular Kondo system while, at higher copper concentration ($x = 0.27$), the magnetic moments begin to interact antiferromagnetically with each other through the so-called π -d interaction.

The situation is also rather complex in the phenalenyl-based single-component conductors such as [PLY(O,O)]₂B (see Scheme 1).^{53,54} The radical complex can be substituted by the diamagnetic beryllium analog lacking this extra electron. At low doping levels ($x \leq 0.15$), substitutional doping is effective and increases the conductivity while lowering the activation energy of both compounds. Higher doping proved more difficult as the beryllium analog is not isostructural with its boron congeners, a striking consequence of this different electron count. It has been argued that this effect on the conductivity cannot be described as a classical semiconductor hole doping as the energy levels of the beryllium dopant are not located in the semiconducting gap of the boron complex. The increase in conductivity would rather be a consequence of decreased antiferromagnetic interactions between pairs of boron radicals.

3.6 Alloying effects on magnetic properties

Because of the strong electronic correlations present in these conducting systems (especially in Mott insulators), specific magnetic properties are closely related to these conducting properties and their evolution within solid solutions provide another extremely rich tool to explore phase diagrams. One first example is provided by the TMTTF salts with either AsF_6^- or SbF_6^- .^{74,75} While the AsF_6^- salt exhibits a non-magnetic (Spin-Peierls) ground state below 14 K, the SbF_6^- salt gives rise to an antiferromagnetic ground state below $T_{\text{Néel}} = 8$ K. At higher temperatures, the resistivity of $(\text{TMTTF})_2\text{SbF}_6$ shows clear evidence of an anomaly around $T_\rho = 154$ K, below which $d\rho/dT$ becomes negative, where ρ is the resistivity. This semiconducting charge-ordered phase (below T_ρ) gradually weakens by alloying with AsF_6^- ,^{74b} but proved to be present at all compositions.⁷⁵ First experiments on $(\text{TMTTF})_2[(\text{AsF}_6)_x(\text{SbF}_6)_{1-x}]$ solid solutions using electron spin resonance (ESR) and magnetic susceptibility have detected the antiferromagnetic phase transition and the spin-gap transition near the pure AsF_6^- and SbF_6^- salts, respectively, that is for $x > 0.8$ or $x < 0.2$, while the absence of any ordered ground state was postulated in the intermediate ($x \approx 0.5$) region.^{74c} ¹³C NMR studies of the ground states and critical behavior in this alloy system for $x = 0.3, 0.5$ and 0.67 suggested however that the antiferromagnetic phase and spin-gap phase are in contact at low temperatures. The $x = 0.5$ alloy is situated on the edge of the spin-gap phase, showing a gradual phase transition and significant critical fluctuations at low temperatures, which can be attributed to the quantum critical effect.

Another example is the alloyed quantum spin liquid system based on salts of $\text{Pd}(\text{dmit})_2$.¹¹² Indeed, the anion radical salt $\text{EtMe}_3\text{Sb}[\text{Pd}(\text{dmit})_2]_2$ is a Mott insulator with a triangular lattice where the spin frustration plays an important role. By changing the cation, the

degree of frustration can be tuned without serious changes in the crystal structure. The magnetic ground state of this Mott system depends on the degree of frustration, characterized by the ratio t'/t of interdimer transfer integrals t and t' (see Figure 6). With the smaller Me_4Sb^+ cation, the salt shows an antiferromagnetic long-range order, while with the larger $\text{Et}_2\text{Me}_2\text{Sb}^+$ cation, the salt shows a non-magnetic charge-ordered state. The alloying of the EtMe_3Sb^+ salt with either Me_4Sb^+ or $\text{Et}_2\text{Me}_2\text{Sb}^+$ cations changes lattice constants⁶⁷ and the degree of frustration continuously. This alloyed system conformed a phase diagram where the quantum spin liquid exists as a “phase” (not a critical “point”) located between the antiferromagnetic phase and the charge order phase as shown in Figure 6.

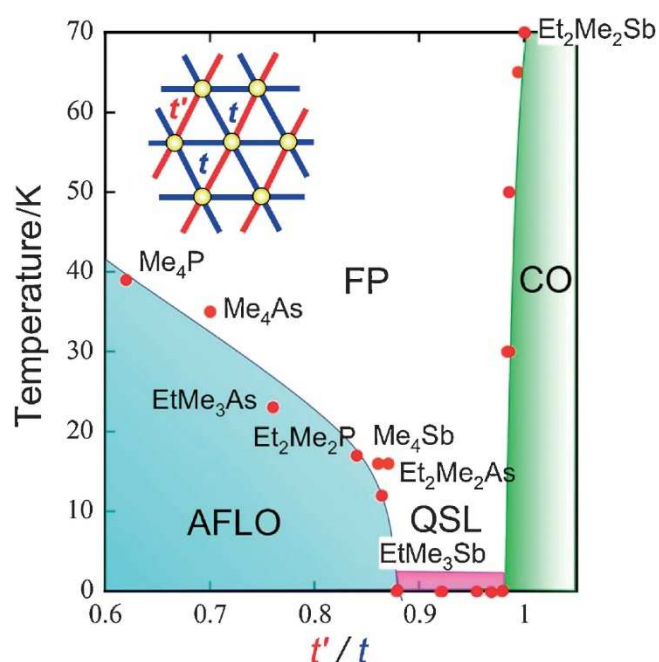


Figure 6. Phase diagram for the series of β' -X[Pd(dmit)₂]₂ salts. Points refereeing to the $(\text{Me}_4\text{Sb})_{1-x}(\text{EtMe}_3\text{Sb})_x[\text{Pd}(\text{dmit})_2]_2$ and $(\text{Et}_2\text{Me}_2\text{Sb})_{1-x}(\text{EtMe}_3\text{Sb})_x[\text{Pd}(\text{dmit})_2]_2$ solid solutions are those located between $t'/t = 0.87$ (for pure Me_4Sb^+ salt) and $t'/t = 1$ (for pure $\text{Et}_2\text{Me}_2\text{Sb}^+$ salt), with the pure EtMe_3Sb^+ salt at $t'/t = 0.92$. Abbreviations: FP, frustrated paramagnetic (state); AFLO, antiferromagnetic long-range ordered (state); CO, charge-ordered (state); QSL, quantum spin liquid (state). Reproduced from Ref. 112 © 2014 The Chemical Society of Japan.

3.7 Magnetic doping

Another sought-after strategy in the elaborations of solid solutions of molecular conductors is the sequential introduction of localized magnetic ions in the neighborhood of a conducting stack. Perhaps one of the first experimental demonstration was reported in the perylene salts $(\text{Per})_2[\text{Pt}_x\text{Au}_{1-x}(\text{mnt})_2]$, where the anionic chains of $[\text{M}(\text{mnt})_2]^-$ complexes are

either diamagnetic ($M = \text{Au}$) or paramagnetic ($M = \text{Pt}$).^{47,48} Both pure compounds, in their α -phase, present a metal-to-insulator transition at 8 K and 12 K respectively that has been ascribed to a Peierls distortion (tetramerisation) of the perylene chains. The Pt compound presents, in addition to the Peierls transition involving the conducting perylene chains, a spin-Peierls transition at the same critical temperature that corresponds to a dimerization of the spin-carrying units $[\text{Pt}(\text{mnt})_2]^-$.¹¹³ This metallic α -phase was still observed in the alloys for $x < 0.50$ or $x > 0.95$ while in the intermediate range $0.50 \leq x \leq 0.95$, the salt adopts another structural β -type associated with a semiconducting behavior on the whole temperature range.⁴⁹

One of the most investigated system along these lines is the λ -(BETS)₂MCl₄ where the diamagnetic GaCl₄⁻ anion can be substituted by the high-spin Fe^{III} FeCl₄⁻ anion ($S = 5/2$).^{92,93} Indeed, λ -(BETS)₂GaCl₄ undergoes a superconducting transition at ≈ 6 K, and the superconductivity is destroyed under a magnetic field of 13 T parallel to the conduction plane. On the other hand, its isostructural analogue λ -(BETS)₂FeCl₄ exhibits a coupled metal-insulator and antiferromagnetic transition at 8.5 K, suggesting the important role of the interaction between the π electrons of BETS and the d electrons of the high-spin Fe³⁺ ion. The insulating phase for λ -(BETS)₂FeCl₄ is destabilized by the magnetic field above ≈ 10 T, where the paramagnetic state of the Fe moments is recovered. A complete phase diagram is shown in Figure 7.

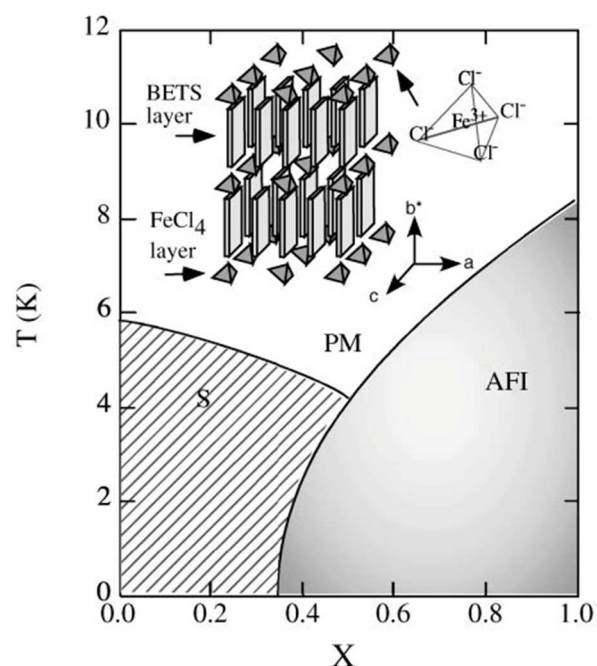


Figure 7 Phase diagram of the organic alloys λ -(BETS) $_2$ Fe $_x$ Ga $_{1-x}$ Cl $_4$ in absence of external magnetic field. PM, AFI and S denote paramagnetic metal, antiferromagnetic insulator and superconductor, respectively. Reproduced from ref 94 ©2003 The Physical Society of Japan.

The field-induced superconductivity for λ -(BETS) $_2$ FeCl $_4$ has been understood in terms of the Jaccarino-Peter effect,¹¹⁴ in which the internal magnetic field due to the exchange interaction with localized Fe moments is crucial. In the (BETS) $_2$ Fe $_x$ Ga $_{1-x}$ Cl $_4$ alloys,⁹⁴ superconductivity is observed only under very high magnetic fields parallel to the conducting layer for $x \geq 0.47$ (Fig. 8). As x decreases, the field induced superconducting phase shifts towards lower fields and a striking field-induced insulator to superconductor transition is observed below 4 T for $x = 0.45$.

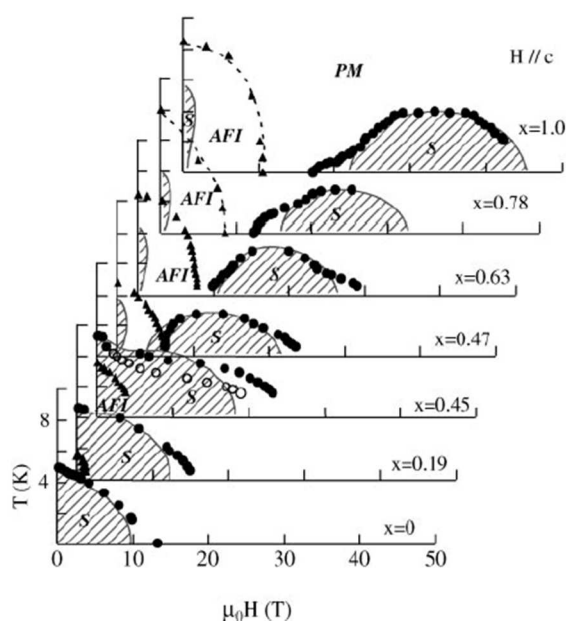


Figure 8 Global magnetic phase diagram of λ -(BETS) $_2$ Fe $_x$ Ga $_{1-x}$ Cl $_4$ under fields applied parallel to the c axis. The PM–S transition fields are defined as the midpoints of the resistive transitions (closed circles), and the AFI– PM or AFI–S transition fields are given by the onset of a sharp change in resistance (triangles). For $x = 0.45$, the onset of the steep change in the PM–S transition is also plotted by opened circles for comparison. The phase boundaries shown by circles and triangles are second and first order transitions, respectively. The shaded areas show the superconducting phases. Reproduced from ref 94 © [2003] The Physical Society of Japan.

4. Conclusions

Solid solution strategies in molecular conductors have been considered since the very beginning of this active research area, as an invaluable tool to modulate, in a continuous way, the structural

and electronic properties of these materials. Such crystalline molecular conductors are characterized by specific properties such as (i) fixed stoichiometry, (ii) low dimensionality, (iii) limited band dispersions, (iv) strong electron correlations and (v) high compressibility. As a consequence, their electronic structure is generally highly sensitive to minute modifications of the solid-state organization, with strong effects of external pressure, but also of composition modifications such as those brought by solid solutions. Both cation and anion radical salts, and single-component conductors have been modified upon alloying and often in the whole composition range, even if novel crystal growth conditions can be needed.

Topics such as preferential insertion and miscibility, nature of disorder and the different analytical tools used for characterizing these alloys have been presented, showing the often-overlooked complexity of these systems. The consequences of alloying on conductivity and on phase transitions (superconductivity, anion ordering, Peierls, Spin-Peierls, antiferromagnetic ground state), the concepts of chemical pressure effects, band filling manipulation, π -d interactions with magnetic anions have been discussed. In many instances however, it proved difficult to sort out which peculiarity of the solid solutions is at the origin of the physical properties' evolution. This complexity makes solid solutions a difficult but extremely rich strategy to also investigate the *electronic* properties of the pure compounds, even if we feel that the *structural* properties of the solid solutions themselves require in most cases deeper investigations.

Conflicts of interest

There are no conflicts to declare.

Acknowledgements

We thank past and current colleagues for interactions on this topic, P. Batail (Orsay, Nantes, Angers), C. Lenoir (Orsay), K. Boubekour (Orsay, Nantes), R. Clérac (Bordeaux), C. Mézière (Nantes, Angers), O. Jeannin (Rennes) and S. Bertaina (Marseille). Financial support is granted by ANR (France) under contract number ANR-20-CE29-0011-02.

Notes and references

- ¹ M. Lusi, *Cryst. Growth Des.*, 2018, **18**, 3704–3712.
- ² S. Aitipamula, R. Banerjee, A. K. Bansal, K. Biradha, M. L. Cheney, A. Roy Choudhury, G. R. Desiraju, A. G. Dikundwar, R. Dubey, N. Duggirala, P. P. Ghogale, S. Ghosh, P. Kumar Goswami, N. Rajesh Goud, R. R. K. R. Jetti, P. Karpinski, P. Kaushik, D. Kumar, V. Kumar, B. Moulton, A. Mukherjee, G. Mukherjee, A. S. Myerson, V. Puri, A. Ramanan, S. T. Rajamannar, C. Malla Reddy, N. Rodriguez-Hornedo, R. D. Rogers, T. N. Guru Row, P. Sanphui, N. Shan, G. Shete, A. Singh, C. C. Sun, J. A. Swift, R. Thaimattam, T. S. Thakur, R. Kumar Thaper, S. P. Thomas, S. Tothadi, V. R. Vangala, N. Variankaval, P. Vishweshwar, D. R. Weyna and M. J. Zaworotko, *Cryst. Growth Des.*, 2012, **12**, 2147–2152.
- ³ X. Huang, X. Liu, K. Ding and S. R. Forrest, *Mater. Horiz.*, 2020, **7**, 244–251.
- ⁴ C. R. Adolf, S. Ferlay and M. W. Hosseini, *CrystEngComm.*, 2018, **20**, 2233–2236.
- ⁵ K. T. Butler, A. Walsch, A. K. Cheetham and G. Kieslich, *Chem. Sci.*, 2016, **7**, 6316–5324.
- ⁶ X. Ding, D. K. Unruh, R. H. Groeneman and K. M Hutchins, *Chem. Sci.*, 2020, **11**, 7701–7707.
- ⁷ F. Brivio, C. Caetano and A. Walsch, *J. Phys. Chem. Lett.*, 2016, **7**, 1083–1087.
- ⁸ M. Habgood, R. Grau-Crespo and S. L. Price, *Phys. Chem. Chem. Phys.*, 2011, **13**, 9590–9600.
- ⁹ J. Bouzaid, M. Schultz, Z. Lao, J. Bartley, T. Bostrom, and J. McMurtrie, *Cryst. Growth Des.*, 2012, **12**, 3906–3916.
- ¹⁰ (a) M. Sorai, J. Ensling and P. Gülich, *Chem. Phys.*, 1976, **18**, 199–209; (b) P. Gülich, R. Link and H.G. Steinhauser, *Inorg. Chem.*, 1978, **17**, 2509–2514; (c) P. Gülich, R. Link, H. Klippen and H.-G. Steinhauser, *J. Chem. Phys.*, 1979, **70**, 3977–3983; (d) O. Kahn and C. J. Martinez, *Science*, 1998, **279**, 44–48.
- ¹¹ T. Tayagaki, A. Galet, G. Molnár, M. C. Muñoz, A. Zwick, K. Tanaka, J.-A. Real, and A. Bousseksou, *J. Phys. Chem. B*, 2005, **109**, 14859–14867.
- ¹² For recent examples, see: (a) F. J. Valverde-Munoz, M. Seredyuk, M. Meneses-Sanchez, M. C. Munoz, C. Bartual-Murguia and J. A. Real, *Chem. Sci.*, 2019, **10**, 3807–3816 ; (b) N. Paradis, F. Le Gac, P. Guionneau, A. Largeteau, D. S. Yufit, P. Rosa, J.-F. Létard and G. Chastanet, *Magnetochemistry*, 2016, **2**, 15 ; (c) M. S. Sylla, C. Baldé, N. Daro, C. Desplanches, M. Marchivie and G. Chastanet, *Eur. J. Inorg. Chem.*, 2018, 297–304 ; (d) C. Bartual-Murgui, C. Pérez-Padilla, S. J. Teat, O. Roubeau and G. Aromí, *Inorg. Chem.*, 2020, **59**, 12132–12142.

- ¹³ S. Chorazy, J. J. Stanek, W. Nogaś, A. M. Majcher, M. Rams, M. Koziel, E. Juszyńska-Gałązka, K. Nakabayashi, S.-i Ohkoshi, B. Sieklucka and R. Podgajny, *J. Am. Chem. Soc.*, 2016, **138**, 1635–1646.
- ¹⁴ J. Wang, Y. Suffren, C. Daignebonne, S. Freslon, K. Bernot, G. Calvez, L. Le Pollès, C. Roiland and O. Guillou, *Inorg. Chem.*, 2019, **58**, 2659–2668.
- ¹⁵ L. M. Aguirre-Díaz, F. Gándara, M. Iglesias, N. Snejko, E. Gutiérrez-Puebla and M. A. Monge, *J. Am. Chem. Soc.*, 2015, **137**, 6132–6135.
- ¹⁶ G. Kieslich, S. Kumagai, A. C. Forse, S. Sun, S. Henke, M. Yamashita, C. P. Grey and T. Cheetham, *Chem. Sci.*, 2016, **7**, 5108–5116.
- ¹⁷ (a) H. Seo, C. Hotta and H. Fukuyama, *Chem. Rev.*, 2004, **104**, 5005–5036 ; (b) T. Giamarchi, *Chem. Rev.*, 2004, **104**, 5037–5055.
- ¹⁸ D. Jérôme, *Chem. Rev.*, 2004, **104**, 5565–5591
- ¹⁹ H. Jiang, P. Hu, J. Ye, K. K. Zhang, Y. Long, W. Hu and C. Kloc, *J. Mater. Chem. C*, 2018, **6**, 1884–1902 and references therein.
- ²⁰ (a) F. Wudl, G. Smith, E. Hufnagel, *J. Chem. Soc. Chem. Commun.*, 1970, 1453–1454; (b) J. Ferraris, D. O. Cowan, W. Walatka, J. Perlstein, *J. Am. Chem. Soc.*, 1973, **95**, 948–949.
- ²¹ T. Mori, *Chem. Rev.*, 2004, **104**, 4947–4969.
- ²² B. A. Scott, S. J. La Placa, J. B. Torrance, B. D. Silverman, and B. Welber, *J. Am. Chem. Soc.*, 1977, **99**, 6631–6639.
- ²³ R. P. Shibaeva, E. B. Yagubskii, *Chem. Rev.*, 2004, **104**, 5347–5378.
- ²⁴ H. Kobayashi, H. B. Cui and A. Kobayashi, *Chem. Rev.*, 2004, **104**, 5265–5288.
- ²⁵ C. Rovira, *Chem. Rev.*, 2004, **104**, 5289–5318.
- ²⁶ (a) S. K. Pal, M. E. Itkis, F. S. Tham, R. W. Reed, R. T. Oakley and R. C. Haddon, *Science*, 2005, **309**, 281–284 ; (b) S. Mandal, S. Samanta, M. E. Itkis, D. W. Jensen, R. W. Reed, R. T. Oakley, F. S. Tham, B. Donnadieu and R. C. Haddon, *J. Am. Chem. Soc.*, 2006, **128**, 1982–1994.
- ²⁷ (a) M. P. Andrews, A. W. Cordes, D. C. Douglass, R. M. Fleming, S. H. Glarum, R. C. Haddon, P. Marsh, R. T. Oakley, T. T. M. Palstra, L. F. Schneemeyer, G. W. Trucks, R. W. Tycko, J. V. Waszczak, K. M. Young and N. M. Zimmerm, *J. Am. Chem. Soc.*, 1991, **113**, 3559–3568 ; (b) A. W. Cordes, R. C. Haddon, R. G. Hicks, R. T. Oakley, T. T. M. Palstra, L. F. Schneemeyer and J. V. Waszczak, *J. Am. Chem. Soc.*, 1992, **114**, 1729–1732.
- ²⁸ (a) A. A. Leitch, R. W. Reed, C. M. Robertson, J. F. Britten, X. Yu, R. A. Secco and R. T. Oakley, *J. Am. Chem. Soc.*, 2007, **129**, 7903–7914; (b) D. Tian, S. M. Winter, A. Mailman, J. W. L. Wong, W. Yong, H. Yamaguchi, Y. Jia, J. S. Tse, S. Desgreniers, R. A. Secco, S.

- R. Julian, C. Jin, M. Mito, Y. Ohishi and R. T. Oakley, *J. Am. Chem. Soc.*, 2015, **137**, 14136–14148.
- ²⁹ (a) T. Isono, H. Kamo, A. Ueda, K. Takahashi, A. Nakao, R. Kumai, H. Nakao, K. Kobayashi, Y. Murakami and H. Mori, *Nat. Commun.*, 2013, **4**, 1344–1349; (b) A. Ueda, S. Yamada, T. Isono, H. Kamo, A. Nakao, R. Kumai, H. Nakao, Y. Murakami, K. Yamamoto, Y. Nishio and H. Mori, *J. Am. Chem. Soc.*, 2014, **136**, 12184–12192.
- ³⁰ Y. Kobayashi, T. Terauchi, S. Sumi and Y. Matsushita, *Nat. Mater.*, 2017, **16**, 109–114.
- ³¹ (a) H. Tanaka, Y. Okano, H. Kobayashi, W. Suzuki and A. Kobayashi, *Science*, 2001, **291**, 285–287; (b) A. Kobayashi, E. Fujiwara, H. Kobayashi, *Chem. Rev.*, 2004, **104**, 5243–5264; (c) H. B. Cui, H. Kobayashi, S. Ishibashi, M. Sasa, F. Iwase, R. Kato, A. Kobayashi, *J. Am. Chem. Soc.*, 2014, **136**, 7619–7622.
- ³² (a) N. Tenn, N. Bellec, O. Jeannin, L. Piekara-Sady, P. Auban-Senzier, J. Iniguez, E. Canadell and D. Lorcy, *J. Am. Chem. Soc.*, 2009, **131**, 16961–16967; (b) Y. Le Gal, T. Roisnel, P. Auban-Senzier, N. Bellec, J. Iniguez, E. Canadell and D. Lorcy, *J. Am. Chem. Soc.*, 2018, **140**, 6998–7004.
- ³³ (a) H. B. Cui, T. Tsumuraya, T. Miyazaki, Y. Okano and R. Kato, *Eur. J. Inorg. Chem.*, 2014, 3837–3840; (b) H. Hachem, H. B. Cui, T. Tsumuraya, R. Kato, O. Jeannin, M. Fourmigué and D. Lorcy, *J. Mater. Chem. C*, 2020, **8**, 11581–11592.
- ³⁴ E. M. Engler, B. A. Scott, S. Etemad, T. Penney and V. V. Patel, *J. Am. Chem. Soc.*, 1977, **99**, 5909–5916.
- ³⁵ (a) Y. Tomkiewicz, E. M. Engler, T. D. Schultz, *Phys. Rev. Lett.*, 1975, **35**, 456–459; (b) P. M. Chaikin, J. F. Kwak, R. L. Greene, S. Etemadt and E. M. Engler, *Solid State Commun.* 1976, **19**, 1201–1204.
- ³⁶ S. Etemad, E. M. Engler, T. D. Schultz, T. Penney and B. A. Scott, *Phys. Rev. B*, 1978, **17**, 513–528.
- ³⁷ S. Ravy, J. P. Pouget and R. Comes, *J. Phys. I France*, 1992, **2**, 1173–1190.
- ³⁸ P. Alemany, E. Canadell and J.-P. Pouget, *Europhys. Lett.*, 2016, **113**, 27006.
- ³⁹ (a) A. J. Epstein, J. S. Miller, J.-P. Pouget and R. Comès, *Phys. Rev. Lett.*, 1981, **47**, 741–744 ; (b) J.-P. Pouget, R. Comès, A. J. Epstein and J. S. Miller, *Mol. Cryst. Liq. Cryst.*, 1982, **85**, 203–213 ; (c) A. J. Epstein, J. W. Kaufer, H. Rommelmann, I. A. Howard, E. M. Conwell, J. S. Miller, J.-P. Pouget and R. Comès, *Phys. Rev. Lett.*, 1982, **49**, 1037–1041.

- ⁴⁰ C. Coulon, P. Delhaes, J. Amiell, J. P. Manteau, J. M. Fabre and I. Giral, *J. Phys. (Paris)*, 1982, **43**, 1721–1729; (b) J. P. Pouget, R. Moret, R. Comes, G. Shirane, K. Bechgaard and J. M. Fabre, *J. Phys. (Paris) Colloq. C3*, 1983, **44**, 969–975.
- ⁴¹ V. Ilakovac, S. Ravy, J. P. Pouget, C. Lenoir, K. Boubekour, P. Batail, S. Dolanski Babic, N. Biskup, B. Korin-Hamzic, S. Tomic and C. Bourbonnais, *Phys. Rev. B*, 1994, **50**, 7136–7139.
- ⁴² P. Auban-Senzier, C. Lenoir, P. Batail, D. Jérôme and S. Tomic, *Eur. Phys. J. B*, 1999, **7**, 529–532.
- ⁴³ K. Mortensen and E. M. Engler, *Phys. Rev. B*, 1984, **29**, 842–850.
- ⁴⁴ (a) T. Naito, A. Miyamoti, H. Kobayashi, R. Kato, A. Kobayashi, *Chem. Lett.*, 1992, 119–122; (b) T. Naito, K. Bu, A. Miyamoto, H. Kobayashi, H. Saw, R. Kato and A. Kobayashi, *Synth. Metals*, 1993, **56**, 2234–2240.
- ⁴⁵ J. Sasaki, A. Kawamoto and K. Kumagai, *Synth. Metals*, 2003, **137**, 1249–1250.
- ⁴⁶ T. Murata, X.-F. Shao, Y. Nakano, H. Yamochi, M. Uruichi, K. Yakushi, G. Saito and K. Tanaka, *Chem. Mater.*, 2010, **22**, 3121–3132.
- ⁴⁷ M. J. Matos, V. Gama, G. Bonfait and R. T. Henriques, *Synth. Metals*, 1993, **55-57**, 1858–1863.
- ⁴⁸ M. J. Matos, M. Almeida, L. Alcacer, R. T. Henriques, *Synth. Metals*, 1997, **86**, 2089–2090.
- ⁴⁹ M. Matos, G. Bonfait, I. C. Santos, M. L. Afonso, R. T. Henriques and M. Almeida, *Magnetochemistry*, 2017, **3**, 22 (1-13)
- ⁵⁰ K. Mebrouk, W. Kaddour, P. Auban-Senzier, C. Pasquier, O. Jeannin, F. Camerel and M. Fourmigué, *Inorg. Chem.*, 2015, **54**, 7454–7460.
- ⁵¹ B. Zhou, M. Shimamura, E. Fujiwara, A. Kobayashi, T. Higashi, E. Nishibori, M. Sakata, H. B. Cui, K. Takahashi and H. Kobayashi, *J. Am. Chem. Soc.*, 2006, **128**, 3872–3873.
- ⁵² Y. Idobata, B. Zhou, A. Kobayashi and H. Kobayashi, *J. Am. Chem. Soc.*, 2012, **134**, 871–874.
- ⁵³ S. K. Pal, P. Bag, M. E. Itkis, F. S. Tham and R. C. Haddon, *J. Am. Chem. Soc.*, 2014, **136**, 14738–14741.
- ⁵⁴ P. Bag, M. E. Itkis, D. Stekovic, S. K. Pal, F. S. Tham and R. C. Haddon, *J. Am. Chem. Soc.*, 2015, **137**, 10000–10008.
- ⁵⁵ G.-J. Yuan, H. Yang, S.-X. Liu, J.-L. Liu and X. M. Ren, *Dalton Trans.*, 2014, **43**, 11908–11914.
- ⁵⁶ X. M. Ren, T. Akutagawa, S. Noro, S. Nishihara, T. Nakamura, Y. Yoshida and K. Inoue, *J. Phys. Chem. B* **2006**, *110*, 7671–7677

- ⁵⁷ A. Fukaya and R. Kato, *J. Phys. Soc. Jpn.*, 2008, **77**, 094710/1-094710/5
- ⁵⁸ R. Kato, H. Sawa, S. Aonuma, M. Tamura, M. Kinoshita and H. Kobayashi, *Solid State Commun.*, 1993, **85**, 831–835.
- ⁵⁹ A. Kobayashi, R. Kato and H. Kobayashi, *Chem. Lett.*, 1989, 1843–1846.
- ⁶⁰ Y. Nishio, K. Kajita, W. Sasaki, R. Kato, A. Kobayashi and H. Kobayashi, *Solid State Commun.*, 1992, **81**, 473–476.
- ⁶¹ S. Hünig, M. Kemmer, H. Meixner, K. Sinzger, H. Wenner, T. Bauer, E. Tillmanns, F. R. Lux, M. Hollstein, H.-G. Groß, U. Langohr, H.-P. Werner, J. U. von Schütz and H. C. Wolf, *Eur. J. Inorg. Chem.*, 1999, 899–916.
- ⁶² P. Erk, S. Hünig, H. Meixner, H.-J. Gross, U. Langohr, H.-P. Werner, J. U. von Schütz and H. C. Wolf, *Angew. Chem. Int. Ed.*, 1989, 1245–1246.
- ⁶³ (a) A. A. Zakhidov, K. Yakushi, K. Imaeda, H. Inokuchi, K. Kikuchi, S. Suzuki, I. Ikemoto and Y. Achiba, *Mol. Cryst. Liq. Cryst.*, 1992, **218**, 299–306; (b) A. A. Zakhidov, K. Imaeda, A. Ugawa, K. Yakushi, H. Inokuchi, Z. Iqbal, R. H. Baughman, B. L. Ramakrishna and Y. Achiba, *Physica C*, 1991, **185-189**, 411–412.
- ⁶⁴ (a) K. Tanaka, K. Yoshizawa, T. Sato, T. Yamabe, K. Okahara and A. A. Zakhidov, *Solid State Comm.*, 1993, **87**, 1055–1059; (b) K. Tanaka, T. Sato, T. Yamabe, K. Yoshizawa, K. Okahara and A. A. Zakhidov, *Phys. Rev. B*, 1995, **51**, 990–995 .
- ⁶⁵ K. Hiraki and K. Kanoda, *Synth. Metals*, 1997, **86**, 2111–2112.
- ⁶⁶ T. Yamamoto, H. Tajima, J. Yamaura, S. Aonuma and R. Kato, *J. Phys. Soc. Jpn.*, 1999, **68**, 1384–1391.
- ⁶⁷ R. Kato, T. Fukunaga, H. M. Yamamoto, K. Ueda and H. B. Cui, *Physica Status Solidi B*, 2012, **249**, 999–1003.
- ⁶⁸ E. W. Reinheimer, A. Assaf, O. Jeannin, A. Benallouche, P.-T. Nguyen, C. Coulon and M. Fourmigué, *Phys. Status Solidi B*, 2012, **249**, 943–946.
- ⁶⁹ S. Tomic, D. Jérôme, D. Mailly, M. Ribault and K. Bechgaard, *J. Phys. Colloq. France C3*, 1983, **44**, 1075–1079.
- ⁷⁰ S. Ravy, R. Moret, J.-P. Pouget and R. Comes, *Physica B+C*, 1986, **143**, 542–546.
- ⁷¹ V. Ilakovac, S. Ravy, K. Boubekour, C. Lenoir, P. Batail and J. P. Pouget, *Phys. Rev. B*, 1997, **56**, 13878–13887.
- ⁷² (a) N. Joo, P. Auban-Senzier, C.R. Pasquier, P. Monod, D. Jérôme and K. Bechgaard, *Eur. Phys. J. B*, 2004, **40**, 43–48; (b) N. Joo, P. Auban-Senzier, C. R. Pasquier, D. Jérôme and K. Bechgaard, *Europhys. Lett.*, 2005, **72**, 645–651.
- ⁷³ T. Yamaguchi, *Synth. Metals*, 2001, **120**, 1005–1006.

- ⁷⁴ (a) R. Laversanne, J. Amiell, C. Coulon, C. Garrigou-Lagrange and P. Delhaes, *Mol. Cryst. Liq. Cryst.*, 1985, **119**, 317–320; (b) R. L ver   e, C. Coulo , B. G llo , J. P. Pouget and R. Moret, *J. Phys. France Lett.*, 1984, **45**, L393–399; (c) R. L ver   e, J. Amiell and C. Coulon, *Mol. Cryst. Liq. Cryst.*, 1986, **137**, 169–178.
- ⁷⁵ F. Iwase, K. Sugiura, K. Furukawa and T. Nakamura, *Phys. Rev. B*, 2010, **81**, 245126.
- ⁷⁶ M. Allain, C. M zi re, P. Auban-Senzier and N. Avarvari, *Crystals*, 2021, **11**, 386 (1-16)
- ⁷⁷ M. Tokumoto, H. Anzai, K. Murata, K. Kajimura and T. Ishiguro, *Synth. Metals*, 1988, **27** A251–256.
- ⁷⁸ H. Anzai, M. Tokumoto, K. Takahashi and T. Ishiguro, *J. Cryst. Growth*, 1988, **91**, 225–228.
- ⁷⁹ H. Kobayashi, R. Kato, A. Kobayashi, T. Mori and H. Inokuchi. *Solid State Commun.*, 1986, **60**, 473–480.
- ⁸⁰ E. Amberger, H. Fuchs and K. Polborn, *Synth. Metals*, 1987, **19**, 605–610
- ⁸¹ H. Kobayashi, R. Kato, A. Kobayashi, Y. Nishio, K. Kajita and W. Sasaki, *Chem. Lett.*, 1986, **15**, 789–792.
- ⁸² M. Fettouhi, L. Ouahab, D. Grandjean, L. Ducasse, J. Amiell, R. Canet and P. Delhaes, *Chem. Mater.*, 1995, **7**, 461–471.
- ⁸³ (a) V. A. Bondarenko, Yu. V. Sushko, V. I. Barchuk, V. S. Yefanov, V. V. Dyakin, M. A. Tanatar, N. D. Kushch, and E. B. Yagubskii, *Synth. Met.*, 1993, **56**, 2386–2390; (b) Yu. V. Sushko, K. Andres, N. D. Kusch, and E. B. Yagubskii, *Solid State Commun.*, 1993, **87**, 589–592; (c) H. Posselt, H. M ller, K. Andres, Yu. V. Sushko, and G. Saito, *Synth. Met.*, 1995, **70**, 917–918.
- ⁸⁴ D. Faltermeier, J. Barz, M. Dumm, M. Dressel, N. Drichko, B. Petrov, V. Semkin, R. Vlasova, C. M zi re and P. Batail, *Phys. Rev. B*, 2007, **76**, 165113.
- ⁸⁵ S. Yasin, M. Dumm, B. Salameh, P. Batail, C. M zi re and M. Dressel, *Eur. Phys. J. B*, 2011, **79**, 383–390.
- ⁸⁶ H. Mori, T. Okano, S. Tanaka, M. Tamura, Y. Nishio, K. Kajita and T. Mori, *J. Phys. Soc. Jpn.*, 2000, **69**, 1751–1756.
- ⁸⁷ H. Mori, M. Kamiya, M. Haemori, H. Suzuki, S. Tanaka, Y. Nishio, K. Kajita and H. Moriyama, *J. Am. Chem. Soc.*, 2002, **124**, 1251–1260.
- ⁸⁸ A. D. Garlach, J. L. Musfeldt, J. M. Pigos, B. R. Jones, I. Olejniczak, A. Graja, M.-H. Whangbo, J. A. Schlueter, U. Geiser, R. W. Winter and G. L. Gard, *Chem. Mater.* 2002, **14**, 2969–2976.

- ⁸⁹ H. Tanaka, A. Kobayashi, T. Saito, K. Kawano, T. Naito and H. Kobayashi, *Adv. Mater.*, 1996, **8**, 812–815.
- ⁹⁰ H. Akutsu, K. Kato, E. Ojima, H. Kobayashi, H. Tanaka, A. Kobayashi and P. Cassoux, *Phys. Rev. B*, 1998, **58**, 9294–9302.
- ⁹¹ H. Kobayashi, H. Akutsu, E. Arai, H. Tanaka, and A. Kobayashi, *Phys. Rev. B*, 1997, **56**, R8526.
- ⁹² H. Kobayashi, A. Sato, E. Arai, H. Akutsu, A. Kobayashi and P. Cassoux, *J. Am. Chem. Soc.*, 1997, **119**, 12392–12393.
- ⁹³ S. Uji, C. Terakura, T. Terashima, T. Yakabe, Y. Terai, M. Tokumoto, A. Kobayashi, F. Sakai, H. Tanaka and H. Kobayashi, *Phys. Rev. B*, 2002, **65**, 113101.
- ⁹⁴ S. Uji, T. Terashima, C. Terakura, T. Yakabe, Y. Terai, S. Yasuzuka, Y. Imanaka, M. Tokumoto, A. Kobayashi, F. Sakai, H. Tanaka, H. Kobayashi, L. Balicas and J. S. Brooks, *J. Phys. Chem. Jpn.*, 2003, **72**, 369–373.
- ⁹⁵ G. Kawaguchi, M. Maesato, T. Komatsu, T. Imakubo, A. Kiswandhi, D. Graf, and H. Kitagawa, *Chem. Mater.*, 2016, **28**, 7276–7286.
- ⁹⁶ M. Katsuhara, M. Aragaki, T. Mori, Y. Misaki and K. Tanaka, *Chem. Mater.*, 2000, **12**, 3186–3191.
- ⁹⁷ M. Katsuhara, M. Aragaki, S. Kimura, T. Mori, Y. Misaki and K. Tanaka, *J. Mater. Chem.*, 2001, **11**, 2125–2130.
- ⁹⁸ M. Katsuhara, S. Kimura, T. Mori, Y. Misaki and K. Tanaka, *Chem. Mater.*, 2002, **14**, 458–462.
- ⁹⁹ T. Devic, M. Evain, Y. Moëlo, E. Canadell, P. Auban-Senzier, M. Fourmigué and P. Batail, *J. Am. Chem. Soc.*, 2003, **125**, 3295–3301.
- ¹⁰⁰ P. Batail, K. Boubekur, M. Fourmigué and J.-C. P. Gabriel, *Chem. Mater.*, 1998, **10**, 3005–3015.
- ¹⁰¹ A. Kitaigorodskii, *Mixed crystals*, Springer Verlag : Berlin, 1984.
- ¹⁰² K. Sarsuns, A. Berzins and T. Rekis, *Cryst. Growth Des.*, 2020, **20**, 7997–8004.
- ¹⁰³ J. E. Eldridge, C. C. Homes, J. M. Williams, A. M. Kini and H. H. Wang, *Spectrochim. Acta A*, 1995, **51**, 947–960.
- ¹⁰⁴ E. Barthel, G. Quirion, P. Wzietek, D. Jérôme, J. B. Christensen, M. Jørgensen and K. Bechgaard, *Europhys. Lett.*, 1993, **21**, 87–92.
- ¹⁰⁵ M. Yamashita, A. Kawamoto, K. Kumagai, *Synth. Metals*, 2003, **133–134**, 125–127.
- ¹⁰⁶ G. E. Pake, *J. Chem. Phys.*, 1948, **16**, 327–336.
- ¹⁰⁷ A. Kawamoto, K. Miyagawa and K. Kanoda, *Phys. Rev. B*, 1997, **55**, 14140–14143.

- ¹⁰⁸ B. R. McGarvey, M. J. Taylor and D. G. Tuck, *Inorg. Chem.*, 1981, **20**, 2010–2013.
- ¹⁰⁹ R. Kirmse, J. Stach, W. Dietzsch, G. Steimecke, and E. Hoyer, *Inorg. Chem.*, 1980, **19**, 2679–2685.
- ¹¹⁰ J. Stach, R. Kirmse, W. Dietzsch, R. M. Olk, and E. Hoyer, *Inorg. Chem.*, 1984, **23**, 4779–4780
- ¹¹¹ R. Kumai, A. Asamitsu, and Y. Tokura, *J. Am. Chem. Soc.*, 1998, **120**, 8263–8264.
- ¹¹² R. Kato, *Bull. Chem. Soc. Jpn.*, 2014, **87**, 355–374.
- ¹¹³ J.-P. Pouget, P. Foury-Leylekian and M. Almeida, *Magnetochem.*, 2017, **3**, 13 (1–24)
- ¹¹⁴ V. Jaccarino and M. Peter, *Phys. Rev. Lett.* 1962, **9**, 290–292.